Soil formation and weathering in a permafrost environment of the Swiss Alps: a multi-parameter and non-steady-state approach

Zollinger, Barbara ; Alewell, Christine ; Kneisel, Christof ; Brandová, Dagmar ; Petrillo, Marta ; Plötze, Michael ; Christl, Marcus ; Egli, Markus

Abstract: Spatially discontinuous permafrost conditions frequently occur in the European Alps. How soils under such conditionshave evolved and how they may react to climate warming is largely unknown. This study focuses on the comparison of nearby soilsthat are characterised by the presence or absence of permafrost (active-layer thickness: 2–3 m) in the alpine (tundra) and subalpine(forest) range of the Eastern Swiss Alps using a multimethod (geochemical and mineralogical) approach. Moreover, a new non-steady-state concept was applied to determine rates of chemical weathering, soil erosion, soil formation, soil denudation, and soilproduction. Long-term chemical weathering rates, soil formation and erosion rates were assessed by using immobile elements,fine-earth stocks and meteoric10Be. In addition, the weathering index (K + Ca)/Ti, the amount of Fe- and Al-oxyhydroxides and clayminerals characteristics were considered. All methods indicated that the differences between permafrost-affected and non-permafrost-affected soils were small. Furthermore, the soils did not uniformly differ in their weathering behaviour. A tendencytowards less intense weathering in soils that were affected by permafrost was noted: at most sites, weathering rates, the proportionof oxyhydroxides and the weathering stage of clay minerals were lower in permafrost soils. In part, erosion rates were higher atthe permafrost sites and accounted for 79–97% of the denudation rates. In general, soil formation rates (8.8–86.7 t/km2/yr) were inthe expected range for Alpine soils. Independent of permafrost conditions, it seems that the local microenvironment (particularlyvegetation and subsequently soil organic matter) has strongly influenced denudation rates. As the climate has varied since the beginning of soil evolution, the conditions for soil formation and weathering were not stable over time. Soil evolution in high Alpinesettings is complex owing to, among others, spatio-temporal variations of permafrost conditions and thus climate. This makes predictions of future behaviour very difficult.

DOI: https://doi.org/10.1002/esp.4040

Soil formation and weathering in a permafrost environment of the Swiss Alps: a multi-parameter and non-steady-state approach

Barbara Zollinger[a], Christine Alewell[b], Christof Kneisel[c], Dagmar Brandová[a], Marta Petrillo[a], Michael Plötze[d], Marcus Christl[e], Markus Egli[a,*]

[a] Department of Geography, University of Zurich, Winterthurerstrasse 190, 8057 Zurich, Switzerland

[b] Institute of Environmental Geosciences, Department of Environmental Sciences, University of Basel, Bernoullistrasse 30, 4056 Basel, Switzerland

[c] Institute of Geography and Geology, University of Würzburg, Am Hubland, 97074 Würzburg, Germany

[d] Institute for Geotechnical Engineering, ETH Zurich, 8093 Zurich, Switzerland

[e] Laboratory of Ion Beam Physics, ETH Zürich, 8093 Zurich, Switzerland

*Corresponding author. Tel.: +41 44 635 51 14; Fax: +41 44 6356848.

E-mail address: markus.egli@geo.uzh.ch (M. Egli).

Abstract

Spatially discontinuous permafrost conditions frequently occur in the European Alps. How soils under such conditions have evolved and how they may react to climate warming is largely unknown. This study focuses on the comparison of nearby soils that are characterised by the presence or absence of permafrost (active-layer thickness: 2 – 3 m) in the alpine (tundra) and subalpine (forest) range of the Eastern Swiss Alps using a multi-method (geochemical and mineralogical) approach. Moreover, a new non-steady-state concept was applied to determine rates of chemical weathering, soil erosion, soil formation, soil denudation, and soil production. Long-term chemical weathering rates, soil formation and erosion rates were assessed by using immobile elements, fine-earth stocks and meteoric ^{10}Be. In addition, the weathering index (K+Ca)/Ti, the amount of Fe- and Al-oxyhydroxides and clay minerals characteristics were considered. All methods indicated that the differences between permafrost-affected and non-permafrost-affected soils were small. Furthermore, the soils did not uniformly differ in their weathering behaviour. A tendency towards less intense weathering in soils that were affected by permafrost was noted: at most sites, weathering rates, the proportion of oxyhydroxides and the weathering stage of clay minerals were lower in permafrost soils. In part, erosion rates were higher at the permafrost sites and accounted for 79 – 97% of the denudation rates. In general, soil formation rates (8.8 – 86.7 t/km^2/y) were in the expected range for Alpine soils. Independent of permafrost conditions, it seems that the local microenvironment (particularly vegetation and subsequently soil organic matter) has strongly influenced denudation rates. As the climate has varied since the beginning of soil evolution, the conditions for soil formation and weathering were not stable over time. Soil evolution in high Alpine settings is complex owing to, among others, spatio-temporal variations of permafrost conditions and thus climate. This makes predictions of future behaviour very difficult.

Keywords: Alpine soils; soil production; soil denudation; soil erosion; cosmogenic radionuclides (^{10}Be)

1 Introduction

Soils underlain by mountain permafrost occupy approximately 3.5 million km^2 worldwide, which accounts for 14 % of the permafrost affected area worldwide (Bockheim and Munroe, 2014). Permafrost is defined as ground material that remains at temperatures at or below 0 °C for two or more years in succession (Gruber and Häberli, 2009). High-mountain permafrost soils are characterised as 'warm' permafrost with relatively high average surface temperatures (-0.5 – +2 °C) and deep active layers (2 to 8 m) (Bockheim and Munroe, 2014). As the occurrence of permafrost in the European Alps is primarily a function of altitude and aspect, discontinuous permafrost can commonly be found at elevations above 2400 m asl at north-exposed slopes and 2900 m asl at south-facing sites (Nötzli and Gruber, 2005). Additionally, sporadic permafrost can exist below the timberline (< 2200 m asl) in the subalpine climate zone, where dense forest stands influence the local microclimate by shading the soil (Kneisel *et al*., 2000). Even small temperature changes in warm permafrost regions are assumed to have distinct environmental impacts. A general permafrost warming trend of 0.5 to 1°C during the last century has already been estimated on the basis of borehole measurements (Harris *et al*., 2003). Even if deep permafrost degradation may be delayed by decades or centuries, progressive climate warming has already led to an extensive active layer-thickening in the European Alps that has had crucial consequences on geomorphological and ecological processes (Gruber *et al*., 2004). As such, conditions for chemical weathering might change in permafrost-affected soils and regolith due to alterations in the thermal and hydrological soil conditions.

Chemical weathering includes the processes of mineral dissolution or alteration and transformation of initial mineral phases into new secondary minerals such as clay minerals or iron oxides. In cryic environments, chemical weathering was long considered to be a negligible process, whereas physical weathering processes were assumed to be the drivers of soil development with freeze-thaw cycles as their main promoters (Hall *et al*., 2002). Meanwhile, several studies show that even cryic soils can be geochemically highly reactive with respect to weathering, including clay mineral formation and soil organic matter accumulation (Allen *et al*., 2001; Föllmi *et al*., 2009; Mavris *et al*., 2010, 2011). Dahms *et al.* (2012) derived from a 1 My alpine chronosequence that weathering rates and soil production rates are highest at the beginning of soil formation and exponentially decrease with increasing age of the soil. Temperature influences weathering through kinetic controls on the rate of chemical reactions. However, the availability of soil moisture seems to be even more important as it provides the environment for chemical reaction and removes dissolved material from rock and soil (Egli *et al*., 2006, 2008; Dixon *et al*., 2009). The weathering progress can be further positively influenced by physical removal of the surface material, which causes continuous exposure of unweathered and highly reactive mineral surfaces to the weathering environment. Up to a certain threshold value, increasing erosion causes increasing chemical weathering rates (Dixon *et al*., 2012). Von Blanckenburg (2005) even stated that erosional processes are more important determinants for chemical weathering than temperature and/or precipitation. However, there is a disagreement about the form of that relationship. Whereas some authors found a linear relationship between chemical weathering and soil erosion (e.g. von Blanckenburg, 2005), others described such linearity only in the supply-limited case (West *et al*., 2005). West *et al*. (2005) further showed that under kinetic limitation weathering is only approximately proportional to the square root of soil erosion. There is no doubt that temperature (energy) determines mineral and soil weathering

— even in the long-term over thousands of years, as shown by Williams *et al*. (2010). Nevertheless, there is no unanimous agreement whether weathering in cold regions will really be increased by the melting of permafrost: and if not, which other factors will be more dominant (Rasmussen *et al*. 2011; Pokrovsky *et al*., 2012; Barnes *et al*., 2014). As shown by previous investigations in the European Alps (Egli *et al*., 2008), higher temperatures do not necessarily lead to higher weathering rates in cold Alpine regions.

The rates of (long-term, averaged) weathering, erosion and denudation are often determined by measuring the amount of cosmogenic nuclides present (e.g. ^{10}Be). However, this approach mostly requires the assumption that denudation and production are balanced and that the soil thickness remains in steady-state. According to Phillips (2010), the assumption of steady-state conditions for soil, regolith, or weathering profile development may lead to unrealistic representations of the dynamics of pedogenesis and weathering profile evolution. Steady-state assumptions should only be applied on surfaces that have been formed on more or less homogeneous bedrock and have not recently been eroded or subjected to colluvial deposition (Phillips, 2010). Consequently, steady-state assumptions might not be valid for Alpine hillslope soils that developed only 'recently' (ca. last 20 ky) on unconsolidated sedimentary parent material.

The aim of this investigation was to reveal chemical weathering processes of Alpine permafrost soils that developed on silicate parent material by using a multi-parameter and non-steady-state approach. By comparing permafrost soils (active-layer thickness: 2 – 3 m) with nearby non-permafrost soils, the following questions were addressed:

1. Do permafrost and adjacent non-permafrost soils in the Alps differ in chemical weathering-, soil denudation-, formation- and production-rates?
2. How do permafrost soils in the Alps differ in their clay mineral assemblages from non-permafrost soils?

Lower soil temperatures and frozen ground conditions during a large part of the year may reduce the moisture availability in permafrost-influenced soils. We consequently assumed we would find lower rates of chemical weathering and related poorly-developed clay mineralogy at permafrost-affected sites.

2 Theoretical background

2.1. Definition of soil production and soil formation

The terms 'soil production', 'soil formation' and 'soil development' have been given differing meanings in different contexts (Alewell *et al.*, 2015). With respect to soil mass, 'soil production' designates the gross production (Egli *et al.*, 2014) whereas 'soil formation' (or 'soil development') describes the net effect (Figure 1). Usually, soil production is understood to mean the conversion rate of bedrock to soil, predominately caused by the mechanical disruption or physical weathering of bedrock (Heimsath *et al.*, 1997; Minasny *et al.,* 2015). However, assigning the term 'soil production' only to the conversion of bedrock material into soil is incomplete. As soil does not only contain inorganic compounds, the net input of organic compounds must also be considered. Moreover, aeolian additions, which in some parts of the world account for a large part of the soil production, should not be neglected (Muhs *et al.*, 2013). Consequently, we define soil production (P_{soil}; Figure 1) to be the gross production as it includes all changes in mass and volume due to the transformation of the parent material into soil (by chemical and physical weathering processes, mineral transformation), the lowering of the bedrock/parent material – soil boundary (Heimsath *et al.*, 1997), but also atmospheric deposition and net organic matter input:

$$P_{Soil} = TP_{soil} + A + (O - G) \quad (1)$$

where TP_{Soil} = the transformation of the parent material or rock into soil; according to eq. (1),

TP_{soil} is equal to $P_{soil,app}$, A = atmospheric deposition and O = net organic matter input, G = organic matter decay (the variables can be expressed as mm/y or t/km^2).

Furthermore, the term soil formation (Figure 1) describes the 'net' effect as it includes all deepening and building-up processes but also takes account of removals from the soil compartment. According to Egli *et al*. (2014) we regard the terms 'soil formation' and 'soil development' to be synonymous. Soil formation rate (F_{Soil}; t/km^2/y) is the net effect of soil mass changes and is expressed by:

$$F_{Soil} = P_{Soil} - D_{Soil} \quad (2)$$

where P_{Soil} (t/km^2/y) = soil production rate and D_{Soil} (t/km^2/y) = denudation rate. Soil formation can moreover be described as a net mass change over time:

$$F_{soil} = \frac{\partial M}{\partial t} \quad (3)$$

where t (y) = surface age and M (t/km^2) = mass of soil. The most vital processes for organisms take place in the fraction ≤ 2 mm, because rock fragments are usually considered chemically inert for plant growth (cf. Ugolini *et al*., 2001). Within this study 'soil' is referred to all loose organic and (weathered) inorganic surface material having a size < 2 mm (referred to as 'fine earth'; *FE*). The corresponding stock of fine earth (*FE*) in a soil can be determined by:

$$FE_{stock} = \sum_{a=1}^{n} FE_i \, \Delta z_i \rho_i \quad (4)$$

Where FE_{stock} (calculated as kg/m^2 and converted to t/km^2) = the fine earth stock summed up over all soil horizons, FE_i = the proportion or concentration of fine earth, Δz_i (m) = the thickness of layer I and ρ (t/m^3) = soil density. The stock of fine earth in a soil profile helps to estimate the soil formation rate (F_{Soil}), as the net effect of soil mass changes according to eq. 3. Therefore, F_{soil} is estimated by:

$$F_{soil} = \frac{\partial FE_{stock}}{\partial t} \quad (5)$$

Soil production can then be written as:

$$P_{Soil} = F_{Soil} + D_{Soil} \quad (6)$$

with

$$D_{Soil} = W_{soil} + E_{soil} \quad (7)$$

where D_{soil} = denudation rate, i.e. mass lost by physical erosion (E_{soil}) and chemical weathering (W_{soil}; all rates given in t/km^2/y) (Alewell *et al.*, 2015; Egli *et al*., 2014).

2.1. The steady-state approach and its limitations

Calculation of soil production and soil denudation rates based on in situ ^{10}Be

The terrestrial cosmogenic nuclide ^{10}Be is often used to quantify soil production and denudation rates (Stockmann *et al*., 2014; Minasny *et al*., 2015). The calculations are based on the model of Nishiizumi *et al*. (1991). The critical assumption is that the nuclide concentration is at steady-state, i.e. erosion and decay balance production. When this condition is satisfied then steady-state concentrations of ^{10}Be (C_{10Be} in atoms/g) in the material sampled can be calculated as:

$$C_{10Be} = \frac{P(h,\theta)}{\left(\lambda + \frac{(\rho\kappa)}{\Lambda}\right)} \quad (8)$$

where $P(h,\theta)$ (atoms/g/y) = the production rate in the target mineral (quartz) at depth h and slope θ, λ (1/y) = the decay constant, ρ (g/cm^3) = the density of the irradiated material, κ (cm/y) = the denudation rate and Λ (g/cm^2) = the attenuation length. The denudation rate is then equalled to the 'apparent soil production' ($P_{soil,app}$; in this case cm/y) which gives:

$$P_{soil,app} = \frac{\Lambda}{\rho}\left(\frac{P}{C_{10Be}} - \lambda\right) \quad (9)$$

An additional critical point in using eq. 8 and 9 is that they originally refer to quartz and related erosion of a rock boulder (or bedrock). In a soil, mass can be removed, but also added due to lateral accumulation — which is hardly the case on rock boulders.

Calculation of chemical weathering rates based on the chemical depletion fraction

The chemical depletion fraction (CDF) is frequently used to estimate chemical weathering rates (W_{soil}). This factor is defined as (Riebe *et al*., 2001):

$$W_{soil} = CDF \cdot D_{soil} \quad (10)$$

with

$$\frac{W_{soil}}{D_{soil}} = \left(1 - \frac{Zr_{rock}}{Zr_{soil}}\right) = CDF \quad (11)$$

and

$$E_{soil} = (1 - CDF) \cdot D_{soil} \quad (12)$$

where D_{soil} (t/km^2/y) = the total denudation rate (usually calculated using in situ ^{10}Be), E_{soil} (t/km^2/y) = the erosion rate, $(Zr)_{rock}$ (g/kg) = the concentration of Zr in the rock or parent material and $(Zr)_{soil}$ the concentration of Zr in the soil. Zr and Ti are considered to be two of the most immobile and thus weathering-inert elements (almost no output with the soil water) since the minerals zircon and rutile are generally quite insoluble (Chadwick *et al*., 1990; White, 1995). This concept is based on the assumption that both soil depth and the considered soil unit volume are at steady-state. A prerequisite would be isovolumetric weathering and a constant volume during soil formation (Riebe *et al*., 2004). Chemical and biophysical weathering is frequently not isovolumetric: an elementary volume may dilate or collapse during soil evolution (Egli and Fitze, 2000; Anderson et al., 2002).

2.3. The new non-steady-state approach

Calculation of chemical weathering rates considering volumetric changes

Differences in chemical composition of the parent and soil material can be used to derive weathering properties. Using immobile elements (e.g. Ti or Zr), element-specific gains and losses are determined and, in the case of known-age landforms, long-term weathering rates can be calculated (Chadwick *et al.*, 1990; Egli and Fitze, 2000). Volumetric changes assumed to occur during pedogenesis are determined by adopting the classical definition of strain, ε_w:

$$\varepsilon_w = \frac{\Delta z_w}{\Delta z} - 1 \quad (13)$$

or

$$\varepsilon_w = \left(\frac{\rho_p C_{i,p}}{\rho_w C_{i,w}}\right) - 1 \quad (14)$$

where Δz (m) = the columnar height of a representative initial volume of unweathered parent material p, Δz_w (m) = the weathered equivalent height w, $C_{i,p}$ (g/t) = the concentration of the immobile element i in the parent material, $C_{i,w}$ (g/t) = the concentration of the immobile element i in the weathered product and ρ_p and ρ_w (t/m^3) = the bulk densities of the parent material and the weathered soil, respectively. The calculation of the open-system mass transport function $\tau_{j,w}$ is defined by (Chadwick *et al.*, 1990):

$$\tau_{j,w} = \left(\frac{C_{j,w} C_{i,p}}{C_{i,w} C_{j,p}}\right) - 1 \quad (15)$$

where $C_{j,p}$ (g/t) = the concentration of element j in the unweathered parent material and $C_{j,w}$ (g/t) = the concentration of element j in the weathered product. With n soil layers, the calculation of changes in mass of element j related to leaching (chemical weathering) or accumulation over a given depth z is defined by (Egli and Fitze, 2000):

$$\bar{m}_{j,flux(z)} = \sum_{a=1}^{n} C_{j,p}\rho_p \left(\frac{1}{\varepsilon_w + 1}\right) \tau_{j,w} \Delta z_w \quad (16)$$

where $\tau_{j,w}$ = the mass transport function, ε_w = the strain, and Δz_w (m) = the weathered equivalent of the columnar height of a representative elementary volume. The sum of elemental mass fluxes per unit time in oxide forms equals W_{soil} (g/m^2/y or converted to t/km^2/y).

$$W_{soil} = \frac{\partial\left(\sum \bar{m}_{j,flux(z)}\right)}{\partial t} \quad (17)$$

Calculation of soil erosion rates using meteoric ^{10}Be

Maejima *et al.* (2005), Tsai *et al*. (2008) and Egli *et al*. (2010) showed that soil erosion rates can also be estimated on the basis of meteoric ^{10}Be. Knowing the age of landforms using independent dating, soil erosion can be calculated by comparing the effective abundance of ^{10}Be measured in the soil with the theoretically necessary abundance for the expected age. With no erosion, the surface age of a soil is given by:

$$t = -\frac{1}{\lambda} \ln\left(1 - \lambda \frac{N_{exp}}{q}\right) \quad \text{and} \quad N_{exp} = q \frac{e^{-\lambda t} - 1}{-\lambda} \quad (18)$$

where N_{exp} (atoms/cm^2) = expected ^{10}Be inventory in the profile (according to the age of the soil; i.e., accumulated ^{10}Be due to atmospheric deposition in the soil and assuming no erosion), q (atoms/cm^2/y) = annual ^{10}Be deposition rate (calculated according to Monaghan *et al*., 1985/1986; Maejima *et al*., 2005), λ (4.997 x 10^{-7}/y) = decay constant of ^{10}Be and t (y) = surface age. As reported in Egli *et al.* (2010), the ^{10}Be deposition rates are mostly unknown for a specific area and have to be estimated. Maejima *et al.* (2005) showed that the deposition rate of ^{10}Be is primarily a function of the amount of precipitation. Average concentrations of

^{10}Be in rainfall are near 1 – 1.5 × 10^4 atoms/cm^3; values that were confirmed also by other investigations (Vonmoos *et al*., 2006; Heikkilä *et al*., 2008a,b). Graly *et al.* (2011) give values between 0.63 ×10^4 and 2.05 ×10^4 atoms/cm^3 of precipitation.

With soil erosion, equation 18 is extended to:

$$t = -\frac{1}{\lambda}\ln\left(1 - \lambda\frac{N}{q - \rho C_{10Be} f E_{soil}}\right) \quad \text{and} \quad E_{soil} = \frac{1}{\rho f C_{10Be}}\left(\frac{\lambda N}{e^{-\lambda t} - 1} + q\right) \qquad (19)$$

where C_{10Be} (atoms/g) = average ^{10}Be in the top eroding horizon, E_{soil} = soil erosion rate (in this equation as cm/y), f = fine earth fraction and ρ (g/cm^3) = the bulk density of the top horizons. One problem is that C_{10Be} evolves over time. This can approximately be solved by using an average value of C_{10Be} between t = 0 and t (corresponding to ~ 0.5 × $C_{10Be(today)}$) and by assuming that erosion losses are concentrated on the topsoil horizon (e.g. 0 – 20 cm). We have

$$\frac{N_{exp} - N}{t} = \frac{\Delta N}{t} = E(N) \qquad (20)$$

where $E(N)$ (atoms/cm^2/y) = annually amount of eroded ^{10}Be. The annual erosion rate (E_{soil}; cm/y) is then derived as:

$$E_{soil} = \frac{z_{top} E(N)}{N_{top}} \qquad (21)$$

where N_{top} = the inventory of ^{10}Be in the topsoil (having the thickness z_{top}; here: 20cm). To convert erosion rates from cm/y to t/km^2/y, E_{soil} has to be multiplied with soil density and referred to km^2.

For the purpose of comparison, an additional, often applied procedure (Lal, 2001) to estimate erosion rates using meteoric ^{10}Be. Soil erosion (E_{soil}) rate is given by:

$$E_{soil} = z_0 K_E \qquad (22)$$

and:

$$K_E = \frac{N_D}{N_S}\left[\frac{Q + q_a}{N_D}\right] - \lambda \quad (23)$$

where z_0 (cm) = thickness of topsoil horizons (comprising O and A horizon), K_E = first order rate constant for removal of soil from the topsoil layer, N_D (atoms/cm^2) = ^{10}Be inventory in the D layer (= remainder of the soil profile comprising B and C horizons, N_S (atoms/cm^2) = ^{10}Be inventory in topsoil horizons, Q (atoms/cm^2/y) = flux of atmospheric ^{10}Be into the topsoil and q_a (atoms/cm^2/y) = flux of meteoric ^{10}Be.

3 Investigation area

The investigation area was located in the Upper Engadine (Switzerland) (Figure 2). The Lateglacial and Holocene history of the Upper Engadine area is well documented (e.g. Suter, 1981; Böhlert *et al*., 2011). The soils are classified as skeleton-rich Cambisols, Cryosols or Podzols (Table 1; IUSS Working Group WRB, 2014). The glacial till consists of granite/gneiss (Julier Granite). According to the Soil Taxonomy (Soil Survey Staff, 2010), the soil moisture regime is udic at all sites and the soil temperature regime is cryic. Maximum precipitation occurs during the summer and autumn months. Two sites in the alpine climate zone (Val Bever, Albula) and one site in the subalpine climate zone (Spinas) were selected (Figure 2, Table 1). Soil ages of 16 ky (Spinas), 11 ky (Val Bever) and 8 ky (Albula) could be derived from independent moraine, peat-bog and rock boulder dating using ^{14}C, in-situ ^{10}Be and geomorphic mapping (Suter, 1981; Böhlert *et al*., 2011).

3.1. Alpine areas (Val Bever and Albula)

These sites are situated at approximately 2700 m a.s.l. For both alpine sites a permafrost distribution map was available (Böckli *et al*., 2012). Furthermore, the occurrence of

permafrost was inferred using two-dimensional geoelectrical soundings and near-surface temperature measurements at the Val Bever sites. Geoelectrical measurements indicated the occurrence of ice-poor permafrost in the bedrock. In general, permafrost was at < 2 – 3 m depth at the Bever site. Permafrost soils are favoured at north-facing slopes, whereas non-permafrost sites are found at south-facing sites. Cryoturbation features, which are common in permafrost soils, could be found at the Val Bever permafrost sites (Figure 2, Table 1). At the Val Bever sites, the permafrost soils had scarce vegetation cover (up to max. 60% soil cover) dominated by the vegetation community Caricetum curvulae (with the exception of one non-permafrost site where the Caricetum curvulae community was also found). The vegetation community Geo Montani-Nardetum dominated the non-permafrost sites and developed a relatively dense vegetation cover (up to 100 %). At the Albula site, the vegetation community Caricetum curvulae dominated the permafrost sites which had a relatively dense vegetation cover compared to the Val Bever site. At the non-permafrost soils, the vegetation consisted of the vegetation communities Caricetum curvulae and Empetro-vaccinetum *(*Ericaceaeous dwarf shrubs).

3.2. Subalpine area (Spinas)

This site was located below the timberline at 1800 m a.s.l. (at present the timberline is between 2200 m and 2300 m a.s.l.) and represents one of the special places at low altitudes where isolated permafrost lenses could be confirmed by geophysical techniques and borehole drilling at lower altitudes (Kneisel *et al*., 2000, 2015). The active layer thickness usually ranged from 2 to 3 m. Mean annual air temperature is 1 °C and the mean annual precipitation is 1050 mm (Böhlert *et al*., 2011). There was no difference in the vegetation cover between the permafrost and non-permafrost soils, except for the dense moss cover at some of the

permafrost sites. The forest community is a Larici-Pinetum cembrae, with blueberry (*Vaccinium myrtillus*) and cranberry (*Vaccinium vitis-idaea*) in the under-storey.

3.3. Experimental set-up and soil sampling

In each area (Val Bever, Spinas, Albula) 3 replicates on permafrost and 3 – 4 replicates on non-permafrost sites were excavated to the C or BC horizon. In total, 19 soil profiles were sampled. The profiles were chosen in a mid-slope position, with the exception of two profiles: at the Albula site one non-permafrost profile was situated in the upper part of the slope ('A1o'; Table 1): at the Val Bever site one permafrost profile was situated on a relatively flat position ('B1m'; Table 1). Soil sampling (bulk soil) was done by horizon. Approximately two to four kilograms of soil was collected per horizon. Soil bulk density was determined using a soil core sampler.

4 Material and methods

4.1. Soil chemistry and physics

Total C and N contents of the soil were measured with a C/H/N analyser (Elementar Vario EL). Soil pH (in 0.01 M $CaCl_2$) was determined on air-dried, fine-earth samples using a soil:solution ratio of 1:2.5. As the soils did not contain inorganic carbon, the total C contents equal the organic carbon content. After a pre-treatment of the samples with H_2O_2 (3%), particle-size distribution of the soils was measured using a combined method consisting of wet-sieving the coarser particles (2000 – 32 µm) and determining the finer particles (< 32 µm) by means of an X-ray sedimentometer (SediGraph 5100). Pedogenic Fe and Al concentrations were determined after treatment of the soil with sodium-dithionite (labelled as 'd', e.g. Fe_d) (McKeague *et al.*, 1971). The dithionite-extraction predominantly separates amorphous, crystalline and organically bound Al- and Fe-oxyhydroxides from the soil

(Borggaard, 1988). By measuring the concentration ratio of the dithionite-extractable Al (Al_d) to Fe (Fe_d) or to the total elemental content (Al_t, Fe_t), soils can be distinguished with respect to their weathering status and age. This means that with increasing age of the soil, more Al is released from the minerals relative to Fe (Fitze, 1982). Consequently, with increasing weathering, the Al_d/Fe_d ratio usually increases. However, the $(Fe_dAl_t)/(Al_dFe_t)$ ratio (decrease with increasing weathering) is more robust as it also considers chemical variations of the total composition of the soil material. The extracts were centrifuged for 8 minutes at 4000 rpm and filtered (mesh size 0.45 µm, S&S, filter type 030/20). Element concentrations were measured using atomic absorption spectrometry (AAnalyst 700, Perkin Elmer). Measurement of the total element content of fine earth and skeleton (i.e. rock fragments > 2mm) was done by means of X-ray fluorescence (XRF). Approximately 5 g of soil material was milled to <50 µm and analysed using an energy dispersive X-ray fluorescence spectrometer (SPECTRO X-LAB 2000, SPECTRO Analytical Instruments, Germany). Total element contents were used to derive chemical weathering rates. In addition, the molar ratio of (K+Ca)/Ti, that was originally applied as a dating tool for rock varnish in semi-arid to arid regions, can be used as a measure for chemical weathering intensities and soil age indicator (Harrington and Whitney, 1987; Böhlert *et al*., 2011; Dahms *et al*., 2012). While K and Ca are easily weathered from the soil column, Ti is considered to be immobile in the soil and is, therefore, passively enriched over time. Consequently, the ratio is lower when the degree of weathering is higher.

Mean ground surface temperature was measured over a period of one year (January 2012 – December 2012) using iButtons (iButton® DS1922L). Ground surface temperatures were measured in the Val Bever area (Table 1; 3 replicates in permafrost and non-permafrost soils; in total 6 sites). Additionally, borehole temperatures were available for the Spinas area (Kneisel *et al*., 2015). In the Val Bever and Spinas area, the volumetric water content was measured using a Time-Domain Reflectometer (TDR) in the immediate radius of the plot (in

July 2013; Table 1). Here, 3 – 4 replicates per site (permafrost, non-permafrost) were analysed (in total: 13 measuring points).

4.2. Clay mineralogy

To separate the clay fraction (< 2 µm), the fine earth samples (< 2 mm, topsoil from 0 – 10 cm soil depth) were pre-treated at room temperature with diluted and Na-acetate buffered (pH 5) H_2O_2 (3%). The clay fraction was obtained by dispersion with Calgon and sedimentation in water. Specimens were then Mg-saturated, washed free of chloride and freeze-dried. Clay samples, orientated on glass slides from a water suspension, were analysed using a Bragg-Brentano Theta-Theta X-ray diffractometer (Bruker AXS D8 Advance) with a Sol-X detector and CoKα-radiation at 40 kV and 30 mA. The device was equipped with primary and secondary soller (4.3°), automatic theta-compensating divergence and antiscatter slits (v18) and a 0.2 mm detector slit. Slides were step-scanned from 2 to 25 °2θ with steps of 0.02 °2θ and a counting time of 2 s/step. The characteristic basal spacing (00l) of clay minerals in orientated specimens were used for qualitative X-ray diffraction analysis after the following treatments: Mg-saturation, ethylene glycol solvation and K saturation, followed by heating for 2 hours to 335 °C and 550 °C. To distinguish the di- and trioctahedral species of clay minerals, the *d*(060) region was measured on randomly-oriented samples step-scanned from 58 to 64 °2θ with steps of 0.02 °2θ at 10 second intervals using a Bruker AXS D8 Advance, Cu-Kα, 4 – 70 °2θ, 40 kV, 40 mA, 0.02 °-steps, 4 s/step, Vantec Detector. Digitised X-ray data were smoothed and corrected for Lorentz and polarisation factors (Moore and Reynolds, 1997). The diffraction patterns in the range of 2 to 15 °2θ and 58 to 64 °2θ were fitted by the Origin™ PFM program using the Pearson VII algorithm. Background values were calculated by means of a non-linear function (polynomial 2nd order function; Lanson, 1997). The

presence of kaolinite was checked using DRIFT analysis (Diffuse Reflectance Infrared Fourier Transform Spectroscopy; OH-stretching region near 3695 cm^{-1}; Bruker, Tensor 27) on powder samples (3% milled soil material, 97 % KBr) heated to 80 °C for ≥ 2 h.

4.3. Analysis of meteoric ^{10}Be and calculation of soil erosion rates

^{10}Be was extracted from the soil samples using a modified method (Egli *et al*., 2010) from Horiuchi *et al*. (1999). 0.4 mg of $^{9}Be(NO_3)_2$ (carrier) was added to 1 – 5 g of soil (< 2 mm fraction). This mixture of carrier and sample was then heated for 3 h at 550 °C to remove organic matter. After cooling, it was put in a shaker and leached with 8 ml HCl (16 % v/v) overnight. The solid part was separated by centrifuge and leached again: the liquid was collected. After a second leaching, the soil residue was disposed of and the obtained solutions mixed together and heated to 80 °C until the volume reduced to c. 1 ml. To this sample, 1 ml HNO_3 (65% v/v) and 1 ml HCl (32 % v/v) were added and any fine particles removed by centrifugation. NaOH (16 % v/v) was added to the sample until it reached a pH value of 2, when 1 ml of conc. EDTA was added. The EDTA solution removes metals (Fe, Mn) in the form of EDTA complexes. NH_4OH was added until a pH value of 8 was obtained and the resulting gel containing $Be(OH)_2$, $Al(OH)_3$ and some $Fe(OH)_2$ and $Mn(OH)_2$ was precipitated. NaOH solution was added to the gel until the pH value reached 14. The $Be(OH)_2$ and $Al(OH)_3$ re-dissolved and the solution containing Be and Al was separated by centrifugation. This procedure was repeated a second time to recover any remaining Be. Once again conc. HCl (32% v/v) was added to the liquid (containing Be) to reach a pH value of 2 and 1 ml of 10 % EDTA was added to remove the last traces of Fe and Mn. The $Be(OH)_2$ and $Al(OH)_3$ were precipitated using NH_4OH and subsequently centrifuged. If Fe was still present, the gel would have been coloured yellow. HCl (32 % v/v) was added until the gel re-dissolved. It was then heated to reduce the volume to c. 1 ml. Any Fe was removed using the

anion exchange column; the cleaned solution was heated to near dryness. The Be and Al were separated using two different cation exchange columns. In the first stage the precipitated gel was dissolved in HCl and passed through the first cation exchange column where most of the Al was adsorbed. After evaporation and precipitation, $Be(OH)_2$ was dissolved in oxalic acid (stage two) and passed through the second cation exchange column that adsorbed the last traces of Al. This second procedure is based on the formation of Al complexes with oxalic acid, and Al is also adsorbed in the column. Pure $Be(OH)_2$ was precipitated using NH_4OH and subsequently dried at 70 °C. It was calcinated in an oven for 2 h at 850 °C to obtain pure BeO. This BeO was then mixed with Cu powder and pressed into a mass spectrometer target. The $^{10}Be/^{9}Be$ ratios were measured at the ETH Zurich Tandem Accelerator Mass Spectrometry (AMS) facility (Kubik and Christl, 2009) using ETH AMS standards S2007N ($^{10}Be/Be = 28.1 \times 10^{-12}$ nominal) and ICN 01-5-1 ($^{10}Be/^{9}Be = 2.709 \times 10^{-11}$ nominal) (Nishiizumi *et al*., 2007) both associated with a ^{10}Be half-life of 1.387±0.012 My.

4.4. Statistics

The normal distribution of the soil chemical data for each study site (including all permafrost and non-permafrost soils) was verified with a Shapiro-Wilk test. A T-Test for data showing homogeneity of variance (F-Test) and Welch-Test for data not showing homogeneity of variance were performed in order to test the difference between the two groups (permafrost, no permafrost). For all tests a level of significance of 0.05 was considered. Statistical analyses were performed using the statistical software R (R development core team 2011, R-Version 2.13.2).

5 Results

5.1. General soil properties

All soils were acidic and the pH ranged from about 3.8 in the topsoil up to 4.6 in the deeper soil horizons (Table 2). The lower horizons and parent material (granitic till) consisted of loamy sand to sandy loam, whereas in the topsoil a higher silt and clay content could be measured. Even at very high altitudes (around 2700 m asl) rather well-developed soil profiles were found having a relatively high concentrations of soil organic carbon at both types of sites (up to 96 g/kg in permafrost soils and up to 197 g/kg in non-permafrost soils; Table 2). At the Bever site, soil moisture was distinctly higher in the non-permafrost soils compared to the permafrost-influenced soils (Table 1); such differences were not detectable at the Spinas site. In addition, distinct differences in the mean annual soil temperature between permafrost and non-permafrost could be discerned (the permafrost sites having about 2 °C lower temperatures). In the topsoil (0 – 10 cm), soil temperatures were near or below 0 °C for about 9 months per year at the permafrost-affected sites (Kneisel *et al*., 2015; Zollinger *et al*., 2015). Borehole temperatures at the Spinas site indicated permafrost conditions at a low depth (Table 1).

5.2. Variable response of chemical weathering rates and weathering indices to permafrost

Chemical weathering rates ranged between 3 – 86 t/km^2/y (Table 3). Average chemical weathering rates over all permafrost soils were 21.88 ± 28.25 t/km^2/y and 17.23 ± 6.17 t/km^2/y for non-permafrost sites, respectively. Significant differences in the chemical weathering rates between permafrost and non-permafrost soils could be detected at the Alpine sites Val Bever and Albula when the single sites were compared with each other, although the differences were not consistent. Whereas the Val Bever permafrost soils had lower chemical weathering rates (2.06 ± 5.79 t/km^2/y) compared to the non-permafrost soils (18.26 ± 3.18 t/km^2/y), the opposite was the case for the Albula site: at that site permafrost soils had higher chemical weathering rates (57.16 ± 28.40 t/km^2/y), compared to the non-permafrost soils (14.11 ± 7.60

t/km^2/y). At the Spinas site, the permafrost soils showed a tendency towards lower weathering rates (10.28 ± 4.23 t/km^2/y and 18.96 ± 7.90 t/km^2/y in non-permafrost).

Some soils (Val Bever and Albula) indicated a weak podzolisation with a translocation of Al_d and Fe_d into lower soil horizons (Table 2). Furthermore, different weathering indicators such as Al_d/Fe_d, Fe_d/Fe_t, $(Fe_dAl_t)/(Al_dFe_t)$ ratios and the stocks of dithionite-extractable Al and Fe were used (Figure 3). However, the differences between permafrost and non-permafrost soils were not significant for most sites. The ratios of Fe_d/Fe_t and Fe_dAl_t/Al_dFe_t between the permafrost and non-permafrost soils differed significantly only at the Val Bever site. The Val Bever non-permafrost sites showed a higher Fe_d/Fe_t-ratio (0.13) and lower values of $(Fe_dAl_t)/(Al_dFe_t)$ (1.93) compared to the Val Bever permafrost sites (Fe_d/Fe_t-ratio: 0.06; Fe_dAl_t/Al_dFe_t: 3.11). Consequently, the permafrost soils had a lower degree of weathering compared to the non-permafrost soils. Significant differences in the (K+Ca)/Ti ratio (topsoil, 0 – 10 cm soil depth) were obtained at the Val Bever site (Figure 4) with higher values for the permafrost soils which is indicative for a lower chemical weathering. However, at the alpine site Albula a trend to lower ratios in permafrost soils was discernible. At the subalpine site Spinas no clear differences could be detected (Figure 4). Additionally, with increasing organic carbon concentrations the (K+Ca)/Ti ratio decreased (Figure 5).

5.3. Identification of clay minerals and influence of permafrost

The differences in the clay mineral assemblage between permafrost and non-permafrost sites were small. Although the signals are not that uniform, it seems (see below) that the clay minerals indicated a slightly more advanced weathering stage at the non-permafrost sites.

Val Bever site: In all samples (Mg-saturated), mica was present (1.00 nm peak, Figure 6). The Mg-saturated clay sample from the Val Bever permafrost site exhibited peaks at 1.42, 1.24, 1.00 and 0.71 nm. EG-solvation did not cause a shift of the 1.42 nm peak to 1.7 nm, which

excludes the presence of smectite. After heating to 335 °C a portion of this peak at 1.42 nm slightly shifted towards 1.00 nm, which indicated the presence of hydroxy-interlayered vermiculite (HIV). Consequently, the irregularly interstratified mineral (Mg-saturated: peak at 1.24 nm) is predominantly mica-HIV. With further heating (to 550 °C) the peak at 0.71 nm disappeared, which indicated the presence of kaolinite (d_{002}*); the peak at 1.42 nm persisted, and thus indicated the presence of chlorite. Kaolinite was confirmed with DRIFT (peak at 3694 cm^{-1}). At the Val Bever non-permafrost site, peaks at 2.40, 1.42, 1.22, 1.04 (minor peak), 1.00 and 0.71 nm could be identified. The peaks at 2.40 and 1.22 nm indicate a regularly-interstratified mica-HIV and/or mica-vermiculite (approx. 70 % mica, 30 % vermiculite; Moore and Reynolds, 1997). Following K-saturation no changes in the peak position could be detected. Similar to the permafrost site, no smectite was detected. The heating procedures (335 °C and 550 °C) evidenved that HIV and chlorite ware also present. Kaolinite was again confirmed by DRIFT. One component that was resistant to heating at a position of 1.20 nm was attributed to an irregularly interstratified chlorite-HIV.

Albula site: The XRD-diffraction patterns of the clay fraction of the permafrost and non-permafrost soils were quite similar. The Mg-saturated sample exhibited clear peaks at 2.40, 1.42, 1.21, 1.00 and 0.71 nm. After EG-solvation, the peak positions at 2.40 and 1.21 nm shifted to 2.60 and 1.26 nm, respectively. This shift was due to expandable smectitic layers in a regularly-interstratified clay mineral (mica-smectite). After K-saturation the peak at 1.00 increased substantially, which is typical for vermiculite. With heating to 335 °C (and 550 °C), the peak at 1.42 nm completely collapsed, which indicated the presence of HIV. No chlorite was present. The peak at 0.71 nm can therefore be attributed to kaolinite (d_{001}*).

Spinas site: Some differences in the clay mineralogy between permafrost and non-permafrost could be discerned. The permafrost soils showed peaks (Mg-saturated) at 1.42, 1.23 (minor peak), 1.00, and 0.71 nm. EG-solvation revealed some interstratified chlorite-smectite (3.15

and 1.70 nm; Moore and Reynolds, 1997) and probably also some smectite (without any interstratification). Vermiculite was also detected (relative increase of the 1.00 nm peka after K-saturation) together with HIV highly HIV, HIV-chlorite (peak centred at approx. 1.21 nm that persisted during the heating treatments) and chlorite (peak at 1.42 nm after heating at 550 °C). Kaolinite was again confirmed with DRIFT. The non-permafrost soils had similar minerals. Also here, an expanding clay mineral (interstratified either with chlorite or HIV) was discerned. Compared to the permafrost soil, more vermiculite but less chlorite and mica seemed to be present.

XRD-patterns in the *d*(060) region (between 58° and 64 °2θ) provide information about the presence of di- (between 59 and 61 °2θ and trioctahedral (between 61 and 63 °2θ phases, respectively (Figure 7). The X-ray profile fitting enabled the separation of a quartz peak near 0.1543 nm and trioctahedral species at 0.155 to 0.156 nm and 0.1539 to 0.1541 nm that could be attributed to biotite and chlorite, respectively (Moore and Reynolds, 1997). The peak near 0.1495 nm was attributed to kaolinite. The highest proportion of dioctahedral species was detected at the Albula. It seems that all permafrost-affected soils had a slightly higher proportion of trioctahedral species than the non-permafrost sites. This would indicate that the non-permafrost soils have a (slightly) advanced weathering stage.

5.4. Soil production, formation and denudation rates

At the sites Val Bever and Spinas, ^{10}Be concentrations were generally higher in the non-permafrost soils (Figure 8 a – c). Some ^{10}Be may have migrated within the soil profile due to the acidic conditions. However, this potential migration did not seem to be very pronounced because even in acidic soils ^{10}Be is strongly adsorbed onto oxyhydroxides and soil organic matter (cf. Egli *et al*., 2010). The expected abundance of ^{10}Be was calculated for a theoretical

soil age of 11 ky for the alpine Val Bever sites, 8 ky for the alpine Albula sites and 16 ky for the subalpine Spinas sites, respectively (Suter, 1981; Böhlert *et al*., 2011). Using equations 5 – 7, soil production rates could be calculated. The soil production rates ranged between 33 t/km^2/y and 222 t/km^2/y. At the Val Bever and Spinas sites, a significant difference between permafrost and non-permafrost soils could be detected, with a higher soil production in the permafrost-affected soils.

Soil formation varied between 16.9 ± 5.5 and 55.3 ± 30.5 t/km^2/y (average values; the whole range is: 8.8 – 86.7 t/km^2/y), with the lowest values found for the Spinas site permafrost soils and the highest values for the Albula permafrost soils, respectively (Figure 8e). For each individual site, with the exception of the Val Bever site, no significant differences in soil formation rates between permafrost and non-permafrost soils were determined. In the Val Bever permafrost soils higher soil formation rates were measured. However, the denudation rates differed significantly between the permafrost and non-permafrost soils of each site, except at the Albula site (Figure 8e). In general, higher topsoil organic carbon stocks seemed to reduce denudation rates (Figure 9) due to lower erosion rates at such sites. Mass redistribution greatly varied from net accumulation (Table 4; negative values) to erosion rates of up to 188 t/km^2/y.

5.5. Studying soil formation and weathering using a multi-parameter approach

Chemical weathering rates, weathering indices, clay assemblages and rates of soil production, formation and denudation were calculated to detect differences in element leaching and mineral transformation processes between permafrost and non-permafrost soils. A general agreement has been obtained using the different methods used (Table 5). It seems that thermal conditions (lower soil temperatures and frozen ground conditions during large parts of the year) in permafrost soils exerted an influence on chemical (weathering) and

physical processes (soil erosion). However, the differences between permafrost and non-permafrost conditions were small (with respect to all parameters) and, depending on the considered site, gave partially a mixed and, therefore, not really conclusive signal.

6 Discussion

6.1 Weathering rates and erosion in cold Alpine environments

In general, the extent (kg/m^2) and rates (t/km^2/y; Table 3) of chemical weathering were in the range of already-published results (cf. Egli *et al*., 2003a; Dixon and Thorn, 2005). Chemical weathering data from alpine environments of Sweden, the Pacific Northwest and central Europe often ranged between 5 - 100 t/km^2/y (cf. Dixon and Thorn, 2005). Merely, the Val Bever non-permafrost soils showed chemical weathering rates that were rather low (2.06 ±5.79 t/km^2/y). Considering the erosion rates (Table 4), our measurements are in line with published results for the central European Alps (0.06 – 0.38 mm/y; Norton et al., 2008, 2010). Two different approaches for the calculation of soil erosion rates were compared (Table 4). Whereas the approaches of Lal (2001) and Egli *et al*. (2010) achieved similar results at sites that were subject to soil erosion, the method of Lal (2001) reaches its limit at depositional sites. An accumulation would only be detectable if the ^{10}Be concentrations in the topsoil were to be three orders of magnitude higher (which is impossible). Considering the chemical weathering and soil erosion rates, our results suggest that erosional and depositional sites show different characteristics and, thus, have to be considered separately. At sites showing no accumulation, increasing soil erosion gives rse to higher rates of chemical weathering — particularly at sites having permafrost ($p < 0.05$). Such a relationship has also been observed elsewhere (Dixon and von Blanckenburg, 2012). In order to identify the boundary between supply-limited and kinetically-limited weathering a few studies tried to parameterise the

relationship between chemical weathering and physical erosion, with: $W \propto E^{\lambda}$, where λ is dimensionless. In supply-limited landscapes, with low erosion rates (10^0 – 10^2 t/km^2/y) the relationship between chemical weathering and erosion should be linear with λ approaching 1. In kinetically limited landscapes with higher erosion rates (10^2 – 10^4 t/km^2/y), lower λ values are expected ($\lambda < 1$). Millot *et al*. (2002), for instance, yielded a λ of 0.66 over a continuum from supply to kinetic limited landscapes (10^0 to 5×10^2 t/km^2/y), whereas West *et al*. (2005) reported values of 0.42 in kinetic limited landscapes (10^2 – 10^4 t/km^2/y). In this study, permafrost sites had an average λ value of 0.40 (±0.10) with erosion rates ranging from 99 to 188 t/km^2/y. It seems that silicate weathering in permafrost soils depends on the kinetics of reactions and is, thus, regulated by temperature, runoff and vegetation (Carson and Kirkby, 1972). In contrast, non-permafrost sites showed a λ value that still points to a kinetic limitation but is closer to supply-limited settings (λ = 0.70 ±14; erosion rates: 27 – 97 t/km^2/y). At such sites, the supply of water, acids and (organic) ligands is large relative to the availability of silicate minerals (West *et al*., 2005; Egli *et al*., 2014). Typically, weathering on young surfaces is kinetically controlled, while old surfaces belong to supply-limited regions (Egli *et al*., 2014).

6.2 Weathering indices and clay mineral formation support findings of non-uniform processes

Stocks and ratios of pedogenic oxyhydroxides (Al_d, Fe_d), the (Ka+Ca)/Ti ratio and clay mineralogy gave a similar result to the chemical weathering rates: lower weathering intensities were found in permafrost soils (Val Bever, Spinas). In contrast, weathering intensities were higher in the permafrost soils compared to the non-permafrost sites at the Albula site. At the Val Bever site, the (K+Ca)/Ti ratio indicated that chemical weathering in permafrost-affected soils is less intense compared to non-permafrost sites (Figure 4). But again, at the Albula site the opposite was observed, i.e. a higher weathering intensity in permafrost soils. In addition, the (K+Ca/Ti) ratio showed a strong, negative correlation with

the organic carbon concentration (Figure 5). Especially in cold environments, soil-forming processes seem to be closely connected with organic matter accumulation and released organic ligands and acids (Certini *et al*., 1998; Egli *et al*., 2008).

Differences in the weathering regime between permafrost and non-permafrost soils at some sites were also confirmed by the clay mineralogy. Under permafrost conditions, all investigated soils had a higher proportion of trioctahedral species compared to the non-permafrost sites (Figure 7). With increasing weathering, the proportion of dioctahedral species usually increases at the expense of trioctahedral phases (Carnicelli *et al*., 1997; Egli *et al*., 2003b). If individual clay minerals are considered, then the differences between permafrost and non-permafrost sites become much less evident (Figure 6). Smectites were found in both soil environments (permafrost/non-permafrost) at the Albula site. At the Spinas site precursors of smectite formation (i.e. interstratified minerals having expandable minerals) were detected in permafrost and non-permafrost soils. However, the complete loss of chlorites indicated a more mature weathering state in the non-permafrost soils (Spinas). Smectite is an end-product of chlorite and mica alteration and, therefore, an indicator for favourable (past or on-going) weathering conditions (Righi *et al*., 1999). Chlorite weathers in a first step into hydroxy-interlayered vermiculite. In a second step, Al-removal from the interlayers, enhanced by organic complexing agents and charge reduction of the mineral, leads to the formation of smectite (Egli *et al*., 2003b). As observed in many Alpine regions, mica often transforms with increasing weathering stage into interstratified mica-vermiculite or mica-smectite and then to smectite (Righi *et al*., 1999; Egli *et al*., 2003b). Neither smectite nor expandable clay minerals were found at the Val Bever site. Similar to the Spinas site soils, the Val Bever soils exhibited a lower weathering status at the permafrost sites with respect to clay mineralogy (e.g. less interstratified minerals such as chlorite-HIV).

The weathering of silicates and formation or transformation of minerals theoretically depend

on mineral reactivity, the supply of mineral, water, acid reactants, ligands and an Arrhenius rate law (Lasaga *et al*., 1994; West et al., 2005). Furthermore, vegetation, which is dependent on the temperature and precipitation, influences weathering through the production of acidity and organic ligands and plays an important role in protecting the soil from physical erosion (Figure 9). At the Val Bever site, the vegetation and organic carbon concentration distinctly differed between the permafrost and non-permafrost affected sites (Table 2, Figure 5). This was less the case at the other sites (Albula, Spinas). The vegetation cover at the permafrost-influenced high-Alpine site (Val Bever) was scarce, while non-permafrost sites had, in contrast, a dense grass cover. Surface disturbance processes (cryoturbation, permafrost creep), are additional environmental factors that may reduce plant establishment (Burga *et al*., 2004). A positive feedback exists between plants and moisture availability. Differences in the availability of soil moisture influence plant growth, productivity and decomposition rates. Lower moisture availability was detected in permafrost soils compared to the non-permafrost soil at the alpine Val Bever site (Table 1). It seems that differences in the soil cover, i.e., vegetation and soil texture (Table 2) have influenced water retention and storage capacity and therefore also chemical weathering.

6.3 Soil formation-, production- and denudation-rates using the non-steady state approach

Considering the soil mass (Figure 10) our data fit well to a data compilation of alpine soils (Alewell *et al*., 2015). With surface age, soil mass is increasing. The given trend in Figure 10 displays soil formation. The corresponding rates can be obtained by the derivation of the regression curve. In this case this would be: $y = 2531.4x^{-0.5047}$; with x = surface age and y = soil mass.

In contrast to other authors, we compare in Figure 8e soil formation rates (instead of chemical weathering rates) with total denudation rates using a non-steady state situation. Total

denudation rates are predominantly determined by erosion (as stated above, the overall chemical losses are rather low). Not surprisingly, this comparison shows that with increasing denudation, soil formation rates also decline (Figure 8e). It seems to be quite logical that a high erosion rate leads to rather shallow soils (eq. 2 – 4). With increasing chemical weathering soil formation rates also increase (R^2 = 0.36; $p < 0.05$).

At our investigation area, erosion rates account for 97 % of the total denudation in permafrost soils and 79 % in non-permafrost soils, respectively. According to Dixon and von Blanckenburg (2012), most soils feature a soil erosion rate of 50 to 90% of the total denudation (based on CDF calculations). Soil production rates at the investigated sites ranged from 33 to 222 t/km^2/y (Table 3), with the highest rates obtained in permafrost-affected soils (with the exception of the Albula site). Mainly due to the high erosion rates especially in permafrost soils, relatively high rates of soil production were obtained for these soils. According to Alewell *et al*. (2015) average (over the entire soil development phase) soil production-rates in Alpine regions for soils having an age of approx. 10 ky are close to 105 t/km^2/y. These findings are in the range of previously reported results of alpine and subalpine soils using the SAST approach (Dahms *et al*., 2012; Egli *et al*., 2014).

6.4 Complex soil evolution due to climate variations

We used a multi-parameter approach to cross-check the results when comparing permafrost with non-permafrost soils. The main findings obtained from parameters such as soil formation and erosion rates can now be compared to those from clay mineralogy and weathering indices (Table 5). Whichever parameter is used, the findings are not straightforward. There is a slight tendency towards higher erosion rates at permafrost sites, and thus less time for weathering, and a subsequent slightly less-intense weathering state. Due to the fact that differences between the permafrost-affected and non-permafrost soils are not always that

evident, we must assume that soil evolution at the investigated sites was complex and not always straightforward. It is known that the climate experienced several variations during the late Pleistocene and Holocene. Frauenfelder *et al*. (2001) estimated for the investigation area that the mean annual air temperature was c. 3 – 4 °C lower than modern values during the Younger Dryas and that the lower limit of permafrost was depressed considerably. In the Younger Dryas, permafrost had been present in areas above c. 1950, 2200, 2450 and 2150 m a.s.l. in the north-, east-, south- and west-facing slopes, respectively (i.e. 500 m to 600 m below the present-day limits of discontinuous permafrost; Frauenfelder, 2001; Böhlert *et al*., 2011). A particularly warmer phase was recorded for the Older and Younger Atlantic period when the treeline was 150 – 250 higher than the present-day one (Burga, 1991; Maisch *et al*., 1999). This, furthermore, means that denser vegetation must have existed about 5000 to 8500 y BP even at high-Alpine sites. Also recent climatic changes (little ice age) may have had an impact on permafrost distribution. Consequently, the permafrost distribution and thickness has varied during soil evolution several times and permafrost may have even disappeared at some of the investigated sites during certain periods. This variability in environmental conditions overshadows the expected differences between permafrost and non-permafrost soils.

Such climate variations certainly happened not only in the Swiss Alps. They were registered in the whole Alpine arc and in many mountain regions worldwide (PAGES 2k consortium, 2013; Büntgen and Hellmann, 2014). Consequently, soils in the warm permafrost zone have worldwide similarly experienced variations with respect to soil formation, chemical weathering and soil production.

7 Conclusion

We assumed that the weathering behaviour between Alpine sites with and without permafrost would differ distinctly. However, this assumption seems to be confirmed only partially. The multi-methodological approach we used showed that soil evolution in high Alpine settings seems to be complex owing to, among other things, spatio-temporal variations of permafrost conditions and thus climate during the late Pleistocene and Holocene. These variations overshadowed to some extent differences between present-day permafrost and non-permafrost soils. Chemical weathering rates of these soils were determined using a non-steady-state approach. Permafrost soils seem to be limited by the kinetic of reactions (kinetic-limited), while non-permafrost soils are limited by the availability of minerals (supply-limited). A trend towards increasing rates of chemical weathering with increasing soil erosion rates was obtained. Soil formation as net building up process, however, decreased with increasing denudation using the non-steady-state approach. Denudation rates were predominately determined by erosion rates that account for 97 % of total denudation in permafrost soils and 79 % in non-permafrost soils. Soil formation rates, furthermore, are declining with increasing age and show, in general, plausible values for Alpine soils. Due to the high erosion rates obtained, especially in permafrost soils, relatively high rates of soil production-rates were measured.

Significant differences in chemical weathering rates between permafrost and non-permafrost soils could not be corroborated for all study sites. Indexes such as the relative proportion of pedogenically-formed oxyhydroxides (e.g. expressed by the ratio of Fe_d/Fe_t) or the Al_d/Fe_d ratio indicated that weathering intensity at (present-day) non-permafrost sites is at least equally as high as, or higher than, that at permafrost sites. The (K+Ca)/Ti index confirmed significant differences for one site only (having a lower ratio and a subsequent higher weathering degree for the non-permafrost site). It further showed a good correlation with the organic carbon concentration. At two of the three investigated sites clay mineral formation

seems to be reduced in permafrost soils. In general, a higher proportion of trioctahedral species is typical for the permafrost sites, indicating lower weathering intensities.

The different methods used agreed in general well and confirmed the complex evolution of the soils. The future weathering behaviour of these high Alpine soils strongly depends on their evolution history and site-specific characteristics.

Acknowledgements This research was supported by the Swiss National Science Foundation (SNSF) project grant no. 200021M_134479 and by the Stiftung für wissenschaftliche Forschung an der Universität Zürich (project no. F-75113-02-01). We are grateful to Alan Rogers for the English corrections.

References

Allen CE, Darmody RG, Thorn CE, Dixon JC, Schlyter P. 2001. Clay mineralogy, chemical weathering and landscape evolution in Arctic–Alpine Sweden. *Geoderma* **99**: 277–294. DOI: 10.1016/S0016-7061(00)00075-6

Alewell C, Egli M, Meusburger K. 2015. An attempt to estimate tolerable soil erosion rates by matching soil formation with denudation in Alpine grasslands. *Journal of Soils and Sediments* **15**: 1383–1399. DOI: 10.1007/s11368-014-0920-6

Anderson SP, Dietrich WE, Brimhall Jr. GH. 2002. Weathering profiles, mass-balance analysis, and rates of solute loss: Linkage between weathering and erosion in a small, steep catchment. *Geological Society of America Bulletin* **114**: 1143–1158.

Barnes RT, Williams MW, Parman JN, Hill K, Caine N. 2014. Thawing glacial and permafrost features contribute to nitrogen export from Green Lakes Valley, Colorado Front Range, USA. *Biogeochemistry* **117**: 413–430. DOI: 10.1007/s10533-013-9886-5

Bockheim JG, Munroe JS. 2014. Organic carbon pools and genesis of alpine soils with permafrost: a review. *Arctic, Antarctic, and Alpine Research* **46**: 987–1006. DOI: 10.1657/1938-4246-46.4.987

Böckli L, Brenning A, Gruber S, Noetzli J. 2012. A statistical approach to modelling permafrost distribution in the European Alps or similar mountain ranges. *Cryosphere* **6**: 125–140. DOI: 10.5194/tc-6-125-2012

Böhlert R, Egli M, Maisch M, Brandová D, Ivy-Ochs S, Kubik PW, Haeberli W. 2011. Application of a combination of dating techniques to reconstruct the Lateglacial and early Holocene landscape history of the Albula region (eastern Switzerland). *Geomorphology* **127**: 1–13. DOI: 10.1016/j.geomorph.2010.10.034

Borggaard OK. 1988. Phase indication by selective dissolution techniques. In *Iron in Soils and Clay Minerals*, Stucki JW, Goodman BA, Schwertmann U (eds). D. Reidel Publishing Company: Dordrecht; 83–89.

Büntgen U, Hellmann L. 2014. The Little Ice Age in Scientific Perspective: Cold Spells and Caveats. *Journal of Interdisciplinary History* **44**: 353–368. DOI: 10.1162/JINH_a_00575

Burga CA. 1991. Vegetation history and paleoclimatology of the Middle Holocene: pollen analysis of alpine peat bog sediments, covered formerly by the Rutor Glacier, 2.510 m (Aosta Valley, Italy). *Global Ecology and Biogeography* **1**: 143–150. DOI: 10.2307/2997428

Burga CA, Frauenfelder R, Ruffet J, Hoelzle M, Kääb A. 2004. Vegetation on Alpine rock glacier surfaces: a contribution to abundance and dynamics on extreme plant habitats. *Flora* **199**: 505–515. DOI: 10.1078/0367-2530-00179

Carnicelli S, Mirabella A, Cecchini G, Sanesi G. 1997. Weathering of chlorite to a low charge expandable mineral in a spodosol on the Apennine Mountains—Italy. *Clays and Clay Minerals* **45**: 28–41.

Carson MA, Kirkby MJ. 1972. *Hillslope Form and Process*, Cambridge University Press:

Cambridge UK; 475.

Certini G, Ugolini FC, Corti G, Agnelli A. 1998. Early stages of podzolization under Corsican pine (Pinus nigra Arn. ssp. laricio). *Geoderma* **83**:103–125. DOI: 10.1016/S0016-7061(97)00137-7

Chadwick OA, Brimhall GH, Hendricks DM. 1990. From a black to a grey box – A mass balance interpretation of pedogenesis. *Geomorphology* **3**: 369–390. DOI: 10.1016/0169-555X(90)90012-F

Dahms D, Favilli F, Krebs R, Egli M. 2012. Soil weathering and accumulation rates of oxalate-extractable phases from alpine chronosequences of up to 1 Ma in age. *Geomorphology* **151–152**: 99–113. DOI: 10.1016/j.geomorph.2012.01.021

Dixon JC, Thorn CE. 2005. Chemical weathering and landscape development in mid-latitude alpine environments. *Geomorphology* **67**: 127–145. DOI: 10.1016/j.geomorph.2004.07.009

Dixon JL, Heimsath AM, Amundson R. 2009. The critical role of climate and saprolite weathering in landscape evolution. *Earth Surface Processes and Landforms* **34**: 1507–1521. DOI: 10.1002/esp.1836

Dixon JL, Hartshorn AS, Heimsath AM, DiBiase RA, Whipple KX, 2012. Chemical weathering response to tectonic forcing: a soils perspective from the San Gabriel Mountains, California. *Earth and Planetary Science Letters* **323–324**: 40–49. DOI: 10.1016/j.epsl.2012.01.010

Dixon JL, von Blanckenburg F. 2012. Soils as pacemakers and limiters of global silicate weathering. *Comptes Rendus Geosciences* **344**: 596–609. DOI: 10.1016/j.crte.2012.10.012

EDI (Eidgenössisches Departement des Innern), 1992. *Hydrologischer Atlas der Schweiz*. Landeshydrologie und -geologie, Bern, Switzerland.

Egli M, Fitze P. 2000. Formulation of pedologic mass balance based on immobile elements: a

revision. *Soil Science* **165**: 437–443.

Egli M, Mirabella A, Sartori G, Fitze P. 2003a. Weathering rates as a function of climate: results from a climosequence of the Val Genova (Trentino, Italian Alps). *Geoderma* **111**: 99–121. DOI: 10.1016/S0016-7061(02)00256-2

Egli M, Mirabella A, Fitze P. 2003b. Formation rates of smectites derived from two Holocene chronosequences in the Swiss Alps. *Geoderma* **117**: 81–98. DOI: 10.1016/S0016-7061(03)00136-8

Egli M, Wernli M, Kneisel C, Haeberli W. 2006. Melting glaciers and soil development in the proglacial area Morteratsch (Swiss Alps): I Soil type chronosequence. *Arctic, Antarctic, and Alpine Research* **38**: 499–509. DOI: 10.1657/1523-0430

Egli M, Mirabella A, Sartori G. 2008. The role of climate and vegetation in weathering and clay mineral formation in late Quaternary soils of the Swiss and Italian Alps. *Geomorphology* **102**: 307–324. DOI: 10.1016/j.geomorph.2008.04.001

Egli M, Brandová D, Böhlert R, Favilli F, Kubik P. 2010. ^{10}Be inventories in Alpine soils and their potential for dating land surfaces. *Geomorphology* **119**: 62–73. DOI: 10.1016/j.geomorph.2010.02.019

Egli M, Dahms D, Norton K. 2014. Soil formation rates on silicate parent material in alpine environments: Different approaches–different results? *Geoderma* **213**: 320–333. DOI: 10.1016/j.geoderma.2013.08.016

Fitze P. 1982. Zur Relativdatierung von Moränen aus Sicht der Bodenentwicklung in den kristallinen Zentralalpen. *Catena* **9**: 265-306.

Föllmi KB, Arn K, Hosein R, Adatte T, Steinmann P. 2009. Biogeochemical weathering in sedimentary chronosequences of the Rhône and Oberaar Glaciers (Swiss Alps): rates and mechanisms of biotite weathering. *Geoderma* **151**: 270–281. DOI: 10.1016/j.geoderma.2009.04.012

Frauenfelder R, Haeberli W, Hoelzle M, Maisch M. 2001. Using relict rockglaciers in GIS-based modelling to reconstruct Younger Dryas permafrost distribution patterns in the Err-Julier area, Swiss Alps. *Norsk Geografisk Tidsskrift* **55**: 195–202. DOI: 10.1080/00291950152746522

Graly JA, Reusser LJ, Bierman PR. 2011. Short and long-term delivery rates of meteoric ^{10}Be to terrestrial soils. *Earth and Planetary Science Letters* **302**: 329–336. DOI: 10.1016/j.epsl.2010.12.020

Gruber S, Hoelzle M, Haeberli W. 2004. Permafrost thaw and destabilization of Alpine rock walls in the hot summer of 2003. *Geophysical Research Letters* **31**: L13504. DOI: 10.1029/2004GL020051

Haeberli W, Gruber S. 2009. Mountain permafrost. In *Permafrost Soils*, Margesin R. (ed.). Springer-Verlag: Soil Biology 16, 33, Berlin Heidelberg; chapter 3. DOI: 10.1007/978-3-540-69371-0

Hall K, Thorn CE, Matsuoka N, Prick A. 2002. Weathering in cold regions: some thoughts and perspectives. *Progress in Physical Geography* **26**: 577–603. DOI: 10.1191/0309133302pp353ra

Harrington CD, Whitney JW. 1987. Scanning electron microscope method of rock-varnish dating. *Geology* **15**: 967–970. DOI: 10.1130/0091-7613(1987)15<967:SEMMFR>2.0.CO;2

Harris C, Vonder Mühll D, Isaksen K, Haeberli W, Sollid JL, King L, Holmlund P, Dramis F, Guglielmin M, Palacios D, 2003. Warming permafrost in European mountains. *Global and Planetary Change* **39**, 215–225. DOI: 10.1016/j.gloplacha.2003.04.001

Heikkilä U, Beer J, Feichter J. 2008a. Modeling cosmogenic radionuclides ^{10}Be and ^{7}Be during the Maunder Minimum using the ECHAM5-HAM general circulation model. *Atmospheric Chemistry and Physics* **8**: 2797–2809. DOI: 10.5194/acp-8-2797-2008

Heikkilä U, Beer J, Alfimov V. 2008b. Beryllium-10 and beryllium-7 in precipitation in Dübendorf (440 m) and at Jungfraujoch (3580 m), Switzerland (1998–2005). *Journal of Geophysical Research* **113** : D11104. DOI: 10.1029/2007JD009160

Heimsath AM, Dietrich WE, Nishiizumi K, Finkel RC. 1997. The soil production rate function and landscape equilibrium. *Nature* **388**: 358–361.

Horiuchi K, Minoura K, Kobayashi K, Nakamura T, Hatori S, Matsuzaki H, Kawai T. 1999. Last-glacial to post-glacial ^{10}Be fluctuations in a sediment core from the Academician Ridge, Lake Baikal. *Geophysical Research Letters* **26**: 1047–1050. DOI: 10.1029/1999GL900163

IUSS Working Group WRB, 2014 *World Reference Base for Soil Resources 2014*. World Soil Resources Reports No. 106. FAO, Rome.

Kneisel C, Hauck C, Vonder Mühll D. 2000. Permafrost below the timberline confirmed and characterized by geoelectrical resistivity measurements, Bever Valley, eastern Swiss Alps. *Permafrost and Periglacial Processes* **11**: 295–304. DOI: 10.1002/1099-1530(200012)11:4<295::AID-PPP353>3.0.CO;2-L

Kneisel C. 2010. The nature and dynamics of frozen ground in alpine and subarctic periglacial environments. *The Holocene* **20**: 423–445. DOI: 10.1177/0959683609353432

Kneisel C, Emmert A, Polich P, Zollinger B, Egli M. 2015. Soil geomorphology and frozen ground conditions at a subalpine talus slope with permafrost in the eastern Swiss Alps. *Catena* **133**: 107–118. DOI: 10.1177/0959683609353432

Kubik PW, Christl M. 2009. ^{10}Be and ^{26}Al measurements at the Zurich 6 MV Tandem AMS facility. *Nuclear Instruments and Methods in Physics Research B* **268**: 880–883. DOI: 10.1016/j.nimb.2009.10.054

Lal D. 2001. New nuclear methods for studies of soil dynamics utilizing cosmic ray produced for radionuclides, In *Sustaining the Global Farm*. Stott DE, Mohtar RH, Steinhardt GC.

(Eds.). 10th International Soil Conservation Organization Meeting, Purdue University and USDA-ARS National Soil Erosion Research Laboratory, 1044–1052.

Lanson B. 1997. Decomposition of experimental X-ray diffraction patterns (profile fitting): a convenient way to study clay minerals. *Clays and Clay Minerals* **45**: 132–146.

Lasaga AC, Soler JM, Ganor J, Burch TE, Nagy KL. 1994. Chemical weathering rate laws and global geochemical cycles. *Geochimica et Cosmochimica Acta* **58**: 2361–2386. DOI: 10.1016/0016-7037(94)90016-7

Maejima Y, Matsuzaki H, Higashi T. 2005. Application of cosmogenic ^{10}Be to dating soils on the raised coral reef terraces of Kikai Island, southwest Japan. *Geoderma* **126**: 389–399. DOI: 10.1016/j.geoderma.2004.10.004

Maisch M, Wipf A, Denneler B, Battaglia J, Benz C. 1999. *Die Gletscher der Schweizer Alpen. Gletscherhochstand 1850, aktuelle Vergletscherung, Gletscherschwund-Szenarien.* Schlussbericht NFP 31 Projekt, vdf-Hochschulverlag ETH Zürich.

Mavris C, Egli M, Plötze M, Blum JD, Mirabella A, Giaccai D, Haeberli W. 2010. Initial stages of weathering and soil formation in the Morteratsch proglacial area (Upper Engadine, Switzerland). *Geoderma* **155**: 359–371. DOI: 10.1016/j.geoderma.2009.12.019

Mavris C, Plötze M, Mirabella A, Giaccai D, Valboa G, Egli M. 2011. Clay mineral evolution along a soil chronosequence in an Alpine proglacial area. *Geoderma* **165**: 106–117. DOI: 10.1016/j.geoderma.2011.07.010

McKeague JA, Brydon JE, Miles NM. 1971. Differentiation of forms of extractable iron and aluminium in soils. *Soil Science Society of Amermica Proceedings* **35**: 33–38. DOI: 10.2136/sssaj1971.03615995003500010016x

Millot R, Gaillardet J, Dupre B, Allegre CJ. 2002. The global control of silicate weathering rates and the coupling with physical erosion: New insights from rivers of the Canadian Shield: *Earth and Planetary Science Letters* **96**: 83–98. DOI: 10.1016/S0012–

821X(01)00599–4

Minasny B, Finke P, Stockmann U, Vanwalleghem T, McBratney AB. 2015. Resolving the integral connection between pedogenesis and landscape evolution. *Earth-Science Reviews* **150**: 102–120. DOI: 10.1016/j.earscirev.2015.07.004

Monaghan MC, Krishnaswami S, Turekian KK. 1985/1986. The global average production of ^{10}Be. *Earth and Planetary Science Letters* **76**: 279–287. DOI: 10.1016/0012-821X(86)90079-8

Moore DM, Reynolds Jr. RC. 1997. *X-ray diffraction and the identification and analysis of clay minerals*. 2nd edition. Oxford University Press, New York.

Muhs DR. 2013. The geologic records of dust in the Quaternary. *Aeolian Research* **9**: 3–48. DOI: 10.1016/j.aeolia.2012.08.001

Nishiizumi K, Kohl CP, Arnold JR, Klein J, Fink D, Middleton R. 1991. Cosmic ray produced ^{10}Be and ^{26}Al in Antarctic rocks: exposure and erosion history. *Earth and Planetary Science Letters* **104**: 440–454. DOI: 10.1016/0012-821X(91)90221-3

Nishiizumi K, Imamura M, Caffee MW, Southon JR, Finkel RC, McAninch J. 2007. Absolute calibration of ^{10}Be AMS standards. *Nuclear Instruments and Methods in Physics Research B* **25**: 403–413. DOI: 10.1016/j.nimb.2007.01.297

Norton KP, von Blanckenburg F, Schlunegger F, Schwab M, Kubik PW. 2008. Cosmogenic nuclide-based investigation of spatial erosion and hillslope channel coupling in the transient foreland of the Swiss Alps. *Geomorphology* **95**: 474–486. DOI: 10.1016/j.geomorph.2007.07.013

Norton KP, von Blanckenburg F, Kubik PW. 2010. Cosmogenic nuclide-derived rates of diffusive and episodic erosion in the glacially sculpted upper Rhone Valley, Swiss Alps. *Earth Surface Processes and Landforms* **35**: 651–662. DOI: 10.1002/esp.1961

Nötzli J, Gruber S. 2005. Alpiner Permafrost – Ein Überblick. *Jahrbuch des Vereins zum Schutz der Bergwelt* **70**: 111–121.

PAGES 2k Consortium. 2013 Continental-scale temperature variability during the past two millennia. *nature geoscience* **6**: 339–346. DOI: 10.1038/ngeo1797

Phillips JD. 2010. The convenient fiction of steady-state soil thickness. *Geoderma* **156**: 389–398. DOI: 10.1016/j.geoderma.2010.03.008

Pokrovsky OS, Viers J, Dupré B, Chabaux F, Gaillardet J, Audry S, Prokushkin AS, Shirikova LS, Kirpotin SN, Lapitsky SA, Shevchenko VP. 2012. Biogeochemistry of carbon, major and trace elements in watersheds of northern Eurasia drained to the Arctic Ocean: The change of fluxes, sources and mechanisms under the climate warming prospective. *Comptes Rendus Geoscience* **344**: 663–677. DOI: 10.1007/s10533-012-9790-4

Rasmussen C, Brantley SL, Richter D, Blum A, Dixon J, White A. 2011. Strong climate control on plagioclase weathering in granitic terrain. *Earth and Planetary Science Letters* **301**: 521–530. DOI: 10.1016/j.epsl.2010.11.037

Riebe CS, Kirchner JW, Granger DE, Finkel RC. 2001. Strong tectonic and weak climatic control of long-term chemical weathering rates. *Geology* **29**: 511–514. DOI: 10.1130/0091-7613(2001)029<0511:STAWCC>2.0.CO;2

Riebe CS, Kirchner JW, Finkel RC. 2004. Erosional and climatic effects on long-term chemical weathering rates in granitic landscapes spanning diverse climate regimes. *Earth and Planetary Science Letters* **224**: 547–562. DOI: 10.1016/j.epsl.2004.05.019

Righi D, Huber K, Keller C. 1999. Clay formation and podzol development from postglacial moraines in Switzerland. *Clay Minerals* **34**: 319–332.

Schwarb M, Daly C, Frei C, Schär C. 2000. *Mittlere jährliche Niederschlagshöhe im europäischen Alpenraum 1971-1990*. Hydrologischer Atlas der Schweiz: Blatt 2.6.

Soil Survey Staff. 2010. *Keys to Soil Taxonomy*. 11th edition, USDA (United States Department of Agriculture), NRCS (National Resources Conservation Service), Washington, DC.

Stockmann U, Minasny B, McBratney AB. 2014. How fast does soil grow? *Geoderma* **216**: 48–61. DOI: 10.1016/j.geoderma.2013.10.007

Sommer, M., Gerke, H.H., Deumlich, D., 2008. Modelling soil landscape genesis – A "time split" approach for hummocky agricultural landscapes. *Geoderma* **145**: 480–493. DOI: 10.1016/j.geoderma.2008.01.012

Suter J. 1981. *Gletschergeschichte des Oberengadins: Untersuchungen von Gletscherschwankungen in der Err-Julier-Gruppe*. Dissertation, University of Zurich, Physische Geographie, vol. 2.

Tsai H, Maejima Y, Hseu ZY. 2008. Meteoric ^{10}Be dating of highly weathered soils from fluvial terraces in Taiwan. *Quaternary International* **188**: 185–196. DOI: 10.1016/j.quaint.2007.06.007

Ugolini CF, Corti G, Dufey JE, Agnelli A, Certini G. 2001. Exchangeable Ca, Mg, and K of rock fragments and fine earth from sandstone and siltstone derived soils and their availability to grass. *Journal of Plant Nutrition and Soil Science* **164**: 309–315. DOI: 10.1002/1522-2624(200106)164:3<309::AID-JPLN309>3.0.CO;2-8

von Blanckenburg F. 2005. The control mechanisms of erosion and weathering at basin scale from cosmogenic nuclides in river sediment. *Earth and Planetary Science Letters* **242**: 224–239. DOI: 10.1016/j.epsl.2005.06.030

Vonmoos M, Beer J, Muscheler R. 2006. Large variations in Holocene solar activity: constraints from ^{10}Be in the Greenland Ice Core Project ice core. *Journal of Geophysical Research* **111**: A10105. DOI: 10.1029/2005JA011500

West AJ, Galy A, Bickle MJ. 2005. Tectonic and climatic controls on silicate weathering: *Earth*

and Planetary Science Letters. **235**: 211–228. DOI: 10.1016/j.epsl.2005.03.020

White AF, Blum AE. 1995. Effects of climate on chemical weathering in watersheds: *Geochimica et Cosmochimica Acta* **59**: 729–1747. DOI: 10.1016/0016-7037(95)00078-E

Williams JZ, Bandsra JZ, Pollard D, Brantley SL. 2010. The temperature dependence of feldspar dissolution determined using a coupled weathering-climate model for Holocene-aged loess soils. *Geoderma* **156**: 11–19. DOI: 10.1016/j.geoderma.2009.12.029

Zollinger B, Alewell C, Kneisel C, Meusburger K, Brandová D, Kubik P, Schaller M, Ketterer M, Egli M. 2015. The effect of permafrost on time-split soil erosion using radionuclides (^{137}Cs, $^{239+240}$Pu, meteoric Be) and stable isotopes (δ^{13}C) in the Eastern Swiss Alps. *Journal of Soils and Sediments* **15**: 1400–1419. DOI: 10.1007/s11368-014-0881-9

Table 1. Characteristics of the study sites

Site	Coordinates[1] (N/E)	Elevation (m asl)	Aspect (°N)	Slope (%)	MAAT[2] (°C)	MAP[2] (mm/y)	Water content (vol. %)	MGST[3] °C	Parent material	Vegetation	Soil orders (WRB[4])
Non-permafrost sites: Alpine											
Val Bever											
B1o	46°32'27"/9°47'52"	2695	120	70	-2.6	1250	25 ± 5	3.1; 3.0	Granite/Gneiss (Julier Granite)	Alpine tundra (Geo Montani-Nardetum)	Entic Podzol
B2o	46°32'32"/9°47'53"	2680	120	78	-2.6	1250	26 ± 18	3.0; 3.0	Granite/Gneiss (Julier Granite)	Alpine tundra (Geo Montani-Nardetum)	Haplic Regosol (humic)
B3o	46°32'30"/9°47'54"	2677	120	36	-2.6	1250	20 ± 12	2.9	Granite/Gneiss (Julier Granite)	Alpine tundra (Caricetum curvulae)	Entic Podzol
Albula											
A1o	46°34'33"/9°53'14"	2615	150	70	-2.6	1250	-	-	Granite/Gneiss (Julier Granite)	Alpine tundra (Caricetum curvulae)	Entic Podzol
A2o	46°34'35"/9°53'17"	2577	160	40	-2.6	1250	-	-	Granite/Gneiss (Julier Granite)	Alpine tundra (Caricetum curvulae)	Entic Podzol
A3o	46°34'34"/9°53'17"	2569	160	42	-2.6	1250	-	-	Granite/Gneiss (Julier Granite)	Alpine tundra (Empeto-vaccinetum)	Entic Podzol
Non-permafrost sites: Subalpine											
Spinas											
S1o	46°33'18"/9°51'29"	1820	26	57	1	1000	16 ± 7	-	Granite rich slope deposits	Natural forest (Larici-Pinetum cembrae)	Albic Podzol
S2o	46°33'18"/9°51'29"	1820	26	57	1	1000	20 ± 6	-	Granite rich slope deposits	Natural forest (Larici-Pinetum cembrae)	Albic Podzol
S3o	46°33'18"/9°51'34"	1796	40	46	1	1000	19 ± 11	-	Granite rich slope deposits	Natural forest (Larici-Pinetum cembrae)	Haplic Podzol
Permafrost sites: Alpine											
Val Bever											
B1m	46°32'36"/9°47'57"	2674	30	0	-2.6	1250	12 ± 9	1.2; 1.1	Granite/Gneiss (Julier Granite)	Alpine tundra (Caricetum curvulae)	Cambic Cryosol

B2m	46°32'40"/9°48'1"	2648	30	36	-2.6	1250	7 ± 3	1.1	Granite/Gneiss (Julier Granite)	Alpine tundra (Caricetum curvulae)	Cambic Cryosol
B3m	46°32'39"/9°48'2"	2663	30	30	-2.6	1250	8 ± 5	1.6; 1.4	Granite/Gneiss (Julier Granite)	Alpine tundra (Caricetum curvulae)	Cambic Cryosol
Albula											
A1m	46°34'32"/9°53'14"	2620	70	62	-2.6	1250	-	-	Granite/Gneiss (Julier Granite)	Alpine tundra (Caricetum curvulae)	Cambic Cryosol
A2m	46°34'31"/9°53'16"	2620	55	62	-2.6	1250	-	-	Granite/Gneiss (Julier Granite)	Alpine tundra (Caricetum curvulae)	Cambic Cryosol
A3m	46°34'30"/9°53'16"	2616	50	70	-2.6	1250	-	-	Granite/Gneiss (Julier Granite)	Alpine tundra (Caricetum curvulae)	Cambic Cryosol
Permafrost sites: Subalpine											
Spinas											
S1m	46°33'19"/9°51'29"	1820	20	57	1	1000	17 ± 10	*	Granite rich slope deposits	Natural forest (Larici-Pinetum cembrae)	Haplic Cambisol (Dystric)
S2m	46°33'19"/9°51'29"	1820	20	57	1	1000	17 ± 10	*	Granite rich slope deposits	Natural forest (Larici-Pinetum cembrae)	Haplic Cambisol (Dystric)
S3m	46°33'18/"9°51'33"	1808	40	46	1	1000	20 ± 4	*	Granite rich slope deposits	Natural forest (Larici-Pinetum cembrae)	Haplic Cambisol (Dystric)
S4m	46°33'17"/9°51'33"	1809	40	53	1	1000	11 ± 4	*	Granite rich slope deposits	Natural forest (Larici-Pinetum cembrae)	Haplic Podzol

[1]World geodetic system (WGS84)
[2]MAAT = mean annual air temperature (according to climate station Bever, 1710 m a.s.l. and Kneisel *et al*., 2010), MAP = mean annual precipitation (according to EDI, 1992; Schwarb *et al*., 2000).
[3]Mean ground surface temperature in the active layer (January – December 2012; in total 5 replicates at the Bever area for both, north- and south-facing sites)
* Mean borehole temperatures (close to these sites; Kneisel *et a*l., 2015): surface +0.46 °C, 1m -0.88 °C, 2m -1.00 °C, 3m -0.85 °C, 5m -0.57 °C, 7m -0.33 °C, 8m -0.21 °C
[4]IUSS Working Group WRB (2014)

Table 2. Physical and chemical characteristics of the fine earth (<2mm)

Site	Horizon	Depth (cm)	Sand (g/kg)	Silt (g/kg)	Clay (g/kg)	pH ($CaCl_2$)	C_{org} (g/kg)	N (g/kg)	C/N	Al_d (g/kg)	Fe_d (g/kg)
Non-permafrost sites - Alpine											
Val Bever											
B1o	O	0-10	122	577	301	4.0	197.0	15	13	8.47	3.09
	OE	10-30	565	197	238	4.0	85.4	7.4	12	3.15	4.65
	Bs	30-50	760	214	26	4.3	25.9	3.4	8	2.93	1.96
	C	50-75	875	111	14	4.4	18.2	2.4	8	1.28	0.61
B2o	A	0-10	-	-	-	4.1	99.3	7.7	13	2.20	5.51
	AC	10-30	-	-	-	4.1	63.5	6.2	10	2.97	5.83
	bA	30-50	-	-	-	4.3	47.8	5.0	10	7.94	6.40
	R	>50	-	-	-	-	-	-	-	-	-
B3o	AE1	0-10	-	-	-	3.9	110.0	7.8	14	5.93	4.06
	AE2	10-30	-	-	-	4.1	107.0	7.1	15	9.05	3.21
	Bhs	30-50	-	-	-	4.3	42.2	3.6	12	6.21	3.90
	Bs	50-60	-	-	-	4.5	13.7	2.3	6	3.46	1.49
	C	60-70	-	-	-	4.6	6.1	1.4	4	1.50	0.00
Albula											
A1o	AE	0-10	483	341	176	3.8	33.0	3.0	11	1.70	5.81
	BA	10-20	448	371	180	4.1	15.9	2.3	7	1.95	7.67
	Bhs1	20-40	485	345	170	4.1	15.0	2.1	7	1.70	7.63
	Bhs2	40-60	723	224	52	4.4	27.9	1.9	15	5.70	7.66
	C	60-70	653	305	42	4.5	10.9	0.2	50	1.90	3.61
A2o	AE	0-10	-	-	-	3.8	73.9	5.5	13	2.70	10.00
	Bhs1	10-20	-	-	-	4.4	39.8	4.1	10	3.75	4.60
	Bhs2	20-35	-	-	-	4.2	14.8	2.8	5	2.20	3.77
	C	35-45	-	-	-	4.5	8.7	1.6	5	1.60	3.36
A3o	A	0-10	-	-	-	3.5	79.6	7.4	11	1.40	8.14
	AE	10-20	-	-	-	3.8	43.6	5.1	9	1.80	9.05
	Bh1	20-40	-	-	-	4.2	32.3	3.6	9	3.20	7.70
	Bh2	40-60	-	-	-	4.3	29.2	3.1	9	3.25	6.66
	C	60-75	-	-	-	4.5	13.5	2.5	5	2.60	3.84
Non-permafrost sites - Subalpine											
Spinas											
S1o	E	0-10	728	205	67	4.0	58.4	3.2	18	2.31	8.90
	Bs1	10-20	750	214	36	3.4	49.9	3.8	13	5.41	9.37
	Bs2	20-30	749	220	31	4.3	37.7	2.2	18	6.36	7.39
	Bs3	30-40	778	184	38	4.4	35.1	2.7	13	7.36	8.86
	B	50-60	649	233	118	4.4	31.9	2.7	12	5.64	7.46
	R	>60	-	-	-	-	-	-	-		
S2o	E	0-10	-	-	-	3.8	63.5	5.8	11	1.98	6.38
	Bs1	10-20	-	-	-	4.2	31.0	3.4	9	3.58	6.55
	Bs2	40-50	-	-	-	4.5	19.8	2.3	9	3.59	6.19
	B	70-80	-	-	-	4.4	15.8	2.4	7	1.77	4.48
	R	>80	-	-	-	-	-	-	-		
S3o	A	0-10	-	-	-	3.8	65.7	3.2	21	3.69	9.24
	E	10-20	-	-	-	3.8	91.5	3.7	25	4.55	8.89
	Bh	20-30	-	-	-	3.7	151.5	4.5	34	5.65	7.44

	2A	30-40	-	-	-	3.7	130.0	4.1	32	5.04	6.94
	2E	40-50	-	-	-	3.7	25.3	1.2	21	2.05	4.18
	2Bs	60-100	-	-	-	4.6	29.2	0.7	42	9.71	14.23
	R	>100	-	-	-	-	-	-	-	-	-
Permafrost sites - Alpine											
Val Bever											
B1m	A	0-10	793	130	77	4.5	15.8	3.1	5	1.10	1.64
	Bw1	10-30	848	89	63	4.5	12.8	2.2	6	1.40	0.96
	Bw2	30-50	786	133	81	4.5	20.1	2.6	8	2.50	1.75
	BC	50-60	814	103	83	4.6	11.6	2.1	6	1.50	0.99
	R	>60	-	-	-	-	-	-	-		
B2m	Ah	0-10	589	295	117	4.6	19.6	3.1	6	1.10	1.32
	Bw1	10-30	688	224	88	4.6	12.1	2.6	5	1.20	1.25
	Bw2	30-35	-	-	-	4.6	12.6	1.9	7	1.80	1.06
	Bw3	35-50	656	262	82	4.6	14.9	2.5	6	2.10	0.96
	C	50-80	587	301	113	4.6	12.7	2.3	5	-	-
B3m	Ah	0-10	-	-	-	4.4	29.6	3.8	8	2.80	2.00
	Bw	10-30	-	-	-	4.6	11.5	2.7	4	1.60	1.32
	BC1	30-50	-	-	-	4.7	7.2	1.7	4	1.10	1.10
	BC2	50-60	-	-	-	4.7	6.1	2.0	3	0.90	1.03
	R	>60	-	-	-	-	-	-	-		
Albula											
A1m	A1	0-10	543	293	164	3.9	27.4	2.3	12	1.89	5.21
	A2	10-20	512	332	156	4.0	20.8	1.8	12	2.21	6.05
	AE	20-40	524	313	163	4.1	21.4	1.3	16	2.41	6.06
	Bs	40-80	619	272	109	4.6	22.1	1.2	18	3.83	7.98
	BC	80-100	674	277	49	4.3	6.6	0.3	26	1.77	3.10
	R	>100	-	-	-	-	-	-	-	-	-
A2m	AE1	0-10	-	-	-	3.6	71.2	4.1	18	2.73	10.43
	AE2	10-20	-	-	-	3.9	42.2	3.8	11	2.44	8.16
	Bhs	20-45	-	-	-	4.3	20.4	1.7	12	3.21	7.86
	B	45-80	-	-	-	4.5	10.3	2.4	4	1.96	6.97
	C	80-100	-	-	-	4.6	3.6	0.2	17	1.30	5.89
A3m	A	0-10	-	-	-	3.8	96.4	5.6	17	3.29	9.57
	AE1	10-20	-	-	-	3.9	63.6	3.8	17	3.24	9.77
	AE2	20-35	-	-	-	4.1	55.6	2.7	21	4.15	8.65
	Bhs	35-60	-	-	-	4.5	32.3	1.4	23	6.41	6.16
	C	60-70	-	-	-	4.6	9.8	0.2	42	2.35	3.71
Permafrost sites - Subalpine											
Spinas											
S1m	A	0-10	633	218	149	3.8	40.0	4.3	9	1.25	4.77
	Bw	25-35	611	239	150	4.4	21.3	2.5	9	0.95	2.35
	BC	50-60	622	234	144	4.5	21.3	2.4	9	2.19	4.68
	R	>60	-	-	-	-	-	-	-		
S2m	A	0-10	-	-	-	3.9	64.4	3.5	18	1.06	5.30
	Bw	25-35	-	-	-	4.1	45.2	2.2	21	2.87	7.68
	BC	50-60	-	-	-	4.1	49.0	2.4	20	2.46	7.99
	R	>60	-	-	-	-	-	-	-		
S3m	Ah	0-10	-	-	-	3.5	93.2	5.5	17	1.54	6.51
	Bw1	10-20	-	-	-	4.0	36.6	3.0	12	3.98	7.80
	Bw2	20-30	-	-	-	4.1	32.6	3.0	11	4.04	6.38
	BC1	30-40	-	-	-	4.2	33.2	2.8	12	4.82	7.29

	BC2	40-50	-	-	-	4.3	29.3	2.1	14	4.60	7.24
	C	50-60	-	-	-	4.3	33.1	3	11	4.77	7.29
S4m	AE	0-10	-	-	-	3.9	57.4	2.1	27	-	-
	Bh	10-20	-	-	-	3.9	35.8	0.8	45	-	-
	Bhs1	20-30	-	-	-	4.2	34.3	1.1	31	-	-
	Bhs2	30-40	-	-	-	4.3	39.9	0.7	57	-	-
	Bhs3	40-50	-	-	-	4.3	33.0	0.2	165	-	-
	Bhs4	50-60	-	-	-	4.3	40.5	0.8	51	-	-
	Bs1	60-70	-	-	-	4.3	36.8	0.8	46	-	-
	Bs2	70-90	-	-	-	4.3	20.9	0.6	35	-	-
	R	>90	-	-	-	-	-	-		-	-

2019

Table 3. Net elemental mass balance of the soil profiles. Negative values refer to accumulation and positive values to losses.

Site	Na_2O (kg/m^2)	MgO (kg/m^2)	Al_2O_3 (kg/m^2)	SiO_2 (kg/m^2)	P_2O_5 (kg/m^2)	K_2O (kg/m^2)	CaO (kg/m^2)	MnO (kg/m^2)	Fe_2O_3 (kg/m^2)	W_{soil}[a] ($t/km^2/y$)	D[b] ($t/km^2/y$)	F_{soil}[c] ($t/km^2/y$)	P_{soil}[d] ($t/km^2/y$)
Non-permafrost sites - Alpine													
Val Bever													
B1o	-0.58	-7.66	22.45	149.7	-0.63	3.10	11.40	0.06	0.74	15.69	7.5	25.8	33.3
B2o	4.80	-2.89	33.06	192.8	-0.25	7.52	7.02	0.04	-0.11	22.00	13.8	25.1	38.9
B3o	-0.67	-5.82	17.45	176.2	-0.44	3.85	8.71	0.05	0.63	18.18	10.0	29.4	39.3
Albula													
A1o	1.99	-3.67	19.37	149.0	0.42	-2.45	13.68	0.13	-0.60	22.24	49.5	42.0	91.5
A2o	0.20	-2.04	12.43	88.6	0.09	-3.33	7.16	0.04	0.33	12.94	40.2	18.9	59.1
A3o	-1.21	-3.86	5.19	57.1	0.08	-8.00	9.99	0.06	-1.97	7.17	34.5	34.1	68.6
Non-permafrost sites - Subalpine													
Spinas													
S1o	3.77	-2.05	29.07	176.9	0.23	2.18	7.20	0.09	-0.05	13.58	110.1	16.6	126.7
S2o	1.66	-3.79	39.78	197.8	-0.08	0.19	9.59	-0.01	-0.43	15.27	111.8	27.5	139.3
S3o	11.80	-1.47	59.72	356.0	-0.13	4.36	15.57	0.21	2.61	28.04	124.5	25.6	150.1
Permafrost sites - Alpine													
Val Bever													
B1m	-9.56	-7.51	-12.82	-16.4	-0.08	-3.10	3.12	0.02	0.10	-4.20	94.3	50.5	144.8
B2m	-8.14	-11.30	-4.80	57.8	-0.56	-1.98	2.03	0.02	1.83	3.17	101.7	44.9	146.6
B3m	-5.84	-9.32	3.51	87.9	-0.28	-0.22	1.99	0	1.59	7.21	105.7	47.5	153.2
Albula													
A1m	11.97	-6.66	61.79	366.2	0.41	-5.77	27.98	0.17	1.34	57.18	49.3	86.7	135.9
A2m	12.94	-4.75	92.23	545.7	0.09	4.81	27.44	0.20	5.72	85.55	77.7	53.6	131.2
A3m	2.52	-2.84	26.67	194.2	-0.12	2.42	7.43	0.06	-1.39	28.74	20.8	25.7	46.5
Permafrost sites - Subalpine													
Spinas													
S1m	-0.03	-3.69	17.29	90.5	-0.04	-2.34	4.37	-0.08	-1.76	6.51	194.0	18.1	212.1
S2m	1.54	-2.13	21.49	85.9	-0.71	-2.78	6.24	-0.16	0.62	6.88	194.4	21.1	215.5
S3m	4.29	-3.43	28.68	166.6	0.17	2.73	6.26	0.01	-0.72	12.79	200.3	8.8	209.1
S4m	4.08	-3.23	32.52	199.4	0.37	-2.01	9.85	0.03	-1.96	14.94	202.4	19.7	222.1

[a] Overall chemical weathering rate:

$$W_{soil} = \frac{1}{t}\sum_{a=1}^{n} \bar{m}_{j,flux(oxide)}$$

with $\bar{m}_{j,flux(oxide)}$ = elemental loss (as oxides; kg/m^2) and t = surface age (y)

[b] Total denudation rate ($D_{soil} = W_{soil} + E_{soil}$); values for E_{soil} cf. Table 5
[c] Soil formation rate (eq. 5)
[d] Soil production rate ($P_{soil} = F_{soil} + D_{soil}$)
pos. values = losses
neg. values = gains

Table 4. Long-term soil erosion rates using meteoric ^{10}Be for the alpine (Val Bever and Albula sites) and subalpine (Spinas sites) permafrost and non-permafrost soils. The erosion rates were calculated for an expected soil age of 11 ky for the alpine 'Val Bever' sites, 8 ky for the alpine 'Albula' sites and 16 ky for the subalpine 'Spinas'sites, respectively (Suter, 1981; Böhlert et al., 2011).

Site	Erosion rate (eq. 21) (t/km^2/y)	Erosion rate (eq. 21) (mm/y)	Erosion rate (eq. 23; Lal, 2001) (t/km^2/y)	Erosion rate (eq. 23; Lal, 2001) (mm/y)
alpine site Bever				
non-permafrost	-8	-0.01	34	0.04
permafrost	99	0.07	108	0.08
alpine site Albula				
non-permafrost	27	0.03	73	0.08
permafrost	-8	-0.01	87	0.10
subalpine site Spinas				
non-permafrost	97	0.08	94	0.08
permafrost	188	0.16	129	0.11

pos. values = erosion
neg. values = accumulation

Table 5. Overall comparison using the considered parameters with respect to permafrost and non-permafrost conditions

Site	Conditions	Chemical weathering rates	Soil formation rates	Erosion rates	Chemical weathering based on (Ca+K)/Ti	Chemical weathering based on Al_d/Fe_d; $[Fe_dAl_t]/[Al_dFe_t]$; Fe_d and Al_d stocks; Fe_d/Fe_t	Chemical weathering based on dioctahedral minerals	Chemical weathering based on clay minerals assemblage
Bever	permafrost	-	+	+	-	-	-	-
Albula	permafrost	+	o	-	(+)	o	(-)	o
Spinas	permafrost	o	o	+	o	-	(-)	(-)
Bever	non-permafrost	+	-	-	+	+	+	+
Albula	non-permafrost	-	o	+	(-)	o	(+)	o
Spinas	non-permafrost	o	o	-	o	+	(+)	(+)

+ = increased
o = indifferent
- = lower
() = small differences

Figure captions

Figure 1. General verview of the applied concept, parameters and methods. At each study site (see Figure 2), Val Bever (alpine, 2700 m a.s.l.), Albula (alpine, 2700 m a.s.l.) and Spinas (subalpine, 1800 m a.s.l.), soils with and without permafrost were analysed.

Figure 2. Locations of the sampling sites in the Upper Engadine, close to the village Bever (46°33'8" N, 9°53'20" E), Switzerland. 1. 'Val Bever' (alpine sites with and without permafrost; vegetation: alpine tundra), 2. 'Albula' (alpine sites with and without permafrost; vegetation: alpine tundra), 3. 'Spinas' (subalpine sites with and without permafrost; vegetation: natural forest). The spatial permafrost distribution is according to Böckli et al. (2012).

Figure 3. Average values of the (a) Al_d/Fe_d ratio (dithionite extractable fraction), (b) Fe_d/Fe_t ratio, (c) Fe_dAl_t/Al_dFe_t ratio, in the B-horizon of the permafrost and non-permafrost soils at each study site (alpine: Val Bever, Albula; subalpine: Spinas). (d) and (e) show the Fe_d- and Al_d-stocks, respectively.

Figure 4. Molar ratio of (K+Ca)/Ti of the bulk material of permafrost and non-permafrost soils at each study site (alpine: Val Bever, Albula; subalpine: Spinas) as a function of the soil depth. Data of the parent material ('Julier Granite') are taken from Böhlert et al. (2011).

Figure 5. Molar ratio of (K+Ca)/Ti of the bulk material of permafrost and non-permafrost soils at each study site (alpine: Bever, Albula; subalpine: Spinas) as a function of the organic carbon concentration.

Figure 6. XRD patterns of soil clays (<2 um) of some topsoil-horizons (0–10 cm soil depth) in the permafrost and non-permafrost soils (Val Bever, Albula, Spinas). The XRD-curves were smoothed and corrected for Lorentz and polarization factors. *d*-spacings are given in nm. EG = ethylene glycol solvation, Mg = Mg-saturation, K = K-saturation and corresponding heating treatments.

Figure 7. XRD patterns in the d_{060} region of the soil clays from topsoils (0–10cm soil depth) in the permafrost and non-permafrost soils of the study sites (a) Val Bever, (b) Albula and (c) Spinas. The peak range between 0.1560 and 0.1530 nm was assigned to trioctahedral and the one between 0.1530 and 0.1480 to dioctahedral phases. Given are the measured values (squares), modelled elementary curves and the modelled overall curve.

Figure 8. (a–c) ^{10}Be concentration as a function of soil depth at the investigated sites. (d) Chemical weathering rate as a function of time for the sites: Albula (8 ky), Bever (11 ky) and Spinas (16 ky). (e) Comparison of rates of soil formation (F_{soil}) and denudation (eq. 7: $D_{soil} = E_{soil} + W_{soil}$) in the permafrost and non-permafrost soils (Bever, Albula, Spinas).

Figure 9. Denudation rates as a function of organic carbon stocks in the topsoil (0–10 cm).

Figure 10. Produced soil mass in alpine soils as a function of time (Alewell et al., 2014, modified).

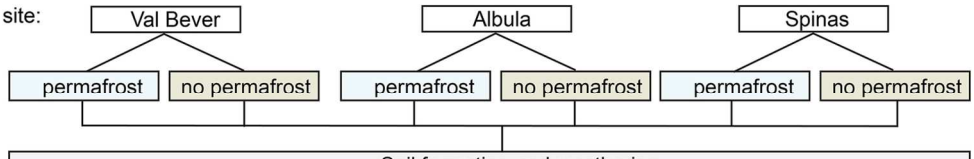

Soil formation and weathering

Symbol	Unit	Process	Method
W_{soil}	t/km²/y	Chemical weathering rate	Mass balance based on immobile elements, consideration of volumetric changes
E_{soil}	t/km²/y	Erosion rate	Comparison of meteoric ^{10}Be inventory with inventory of soil age
D_{soil}	t/km²/y	Denudation rate	$D_{soil} = W_{soil} + E_{soil}$
F_{soil}	t/km²/y	Soil formation rate	Net soil mass changes over time: $F_{soil} = \frac{\partial h}{\partial t} \propto F_{soil} = \frac{\partial M}{\partial t}$
P_{soil}	t/km²/y	Soil production rate	Gross soil mass change over time; $P_{soil} = F_{soil} + D_{soil}$
a) (Ca+K)/Ti		Chemical weathering	Relative enrichment/losses of main elements
b) Fe_d, Al_d		Chemical weathering	Formation of oxyhydroxides (weathering products)
c) Clay mineralogy		Mineral transformation, weathering	Formation of weathering products (clay minerals), proportion of di- to trioctahedral minerals

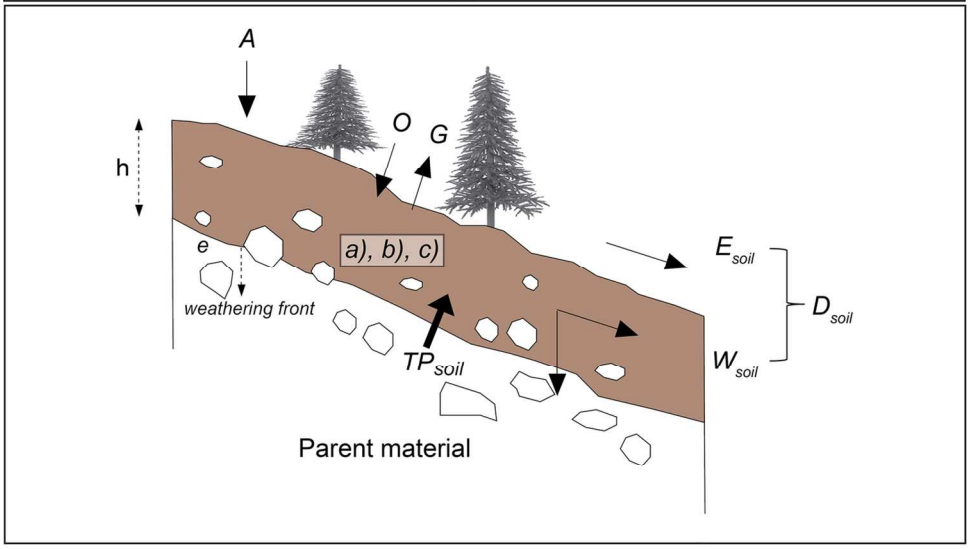

Figure 1

130x154mm (300 x 300 DPI)

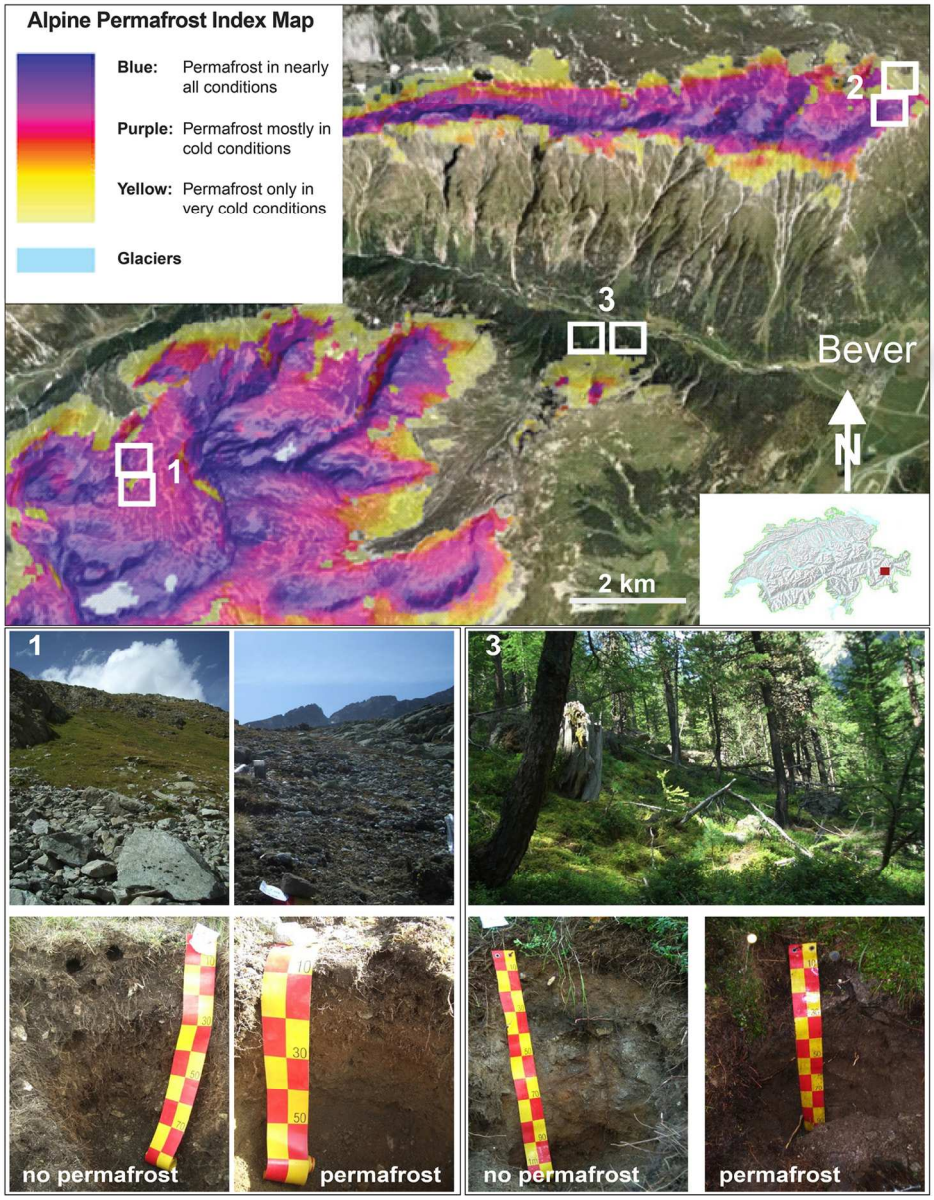

Figure 2

136x170mm (300 x 300 DPI)

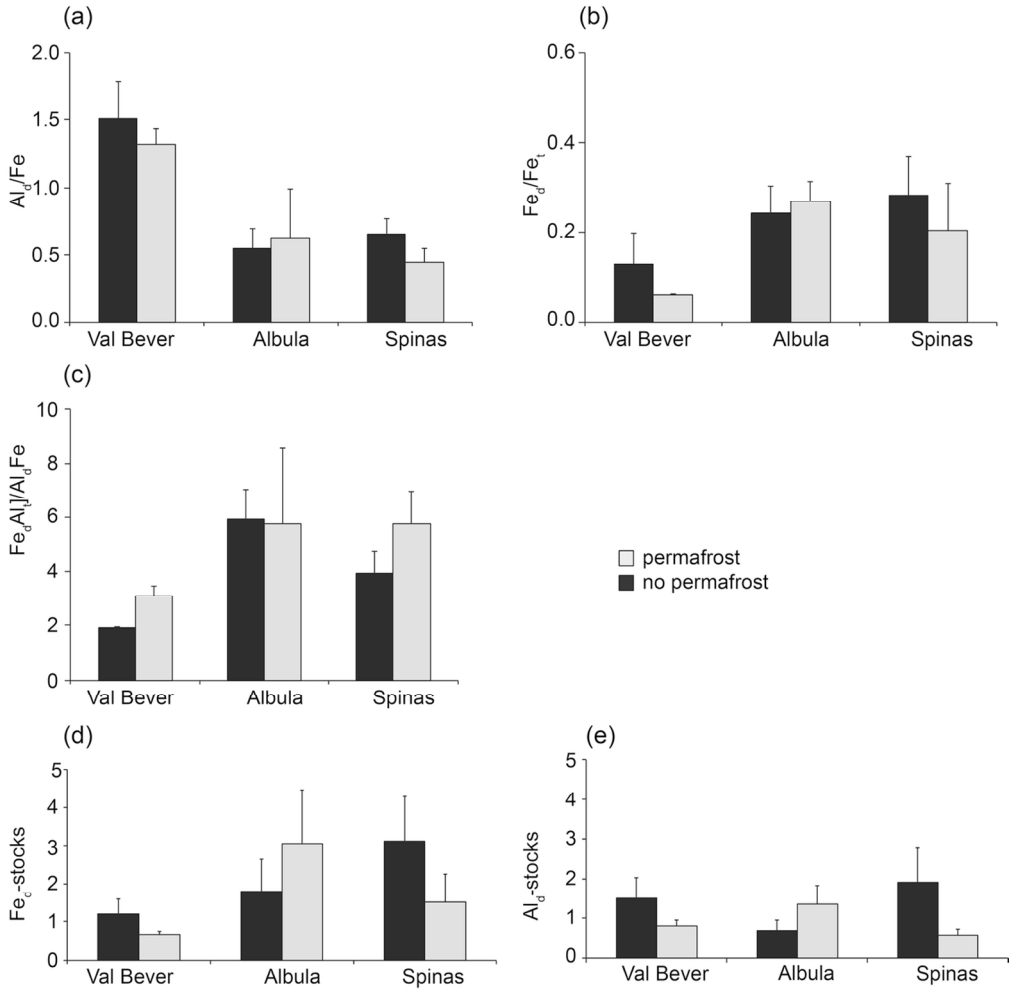

Figure 3

118x116mm (300 x 300 DPI)

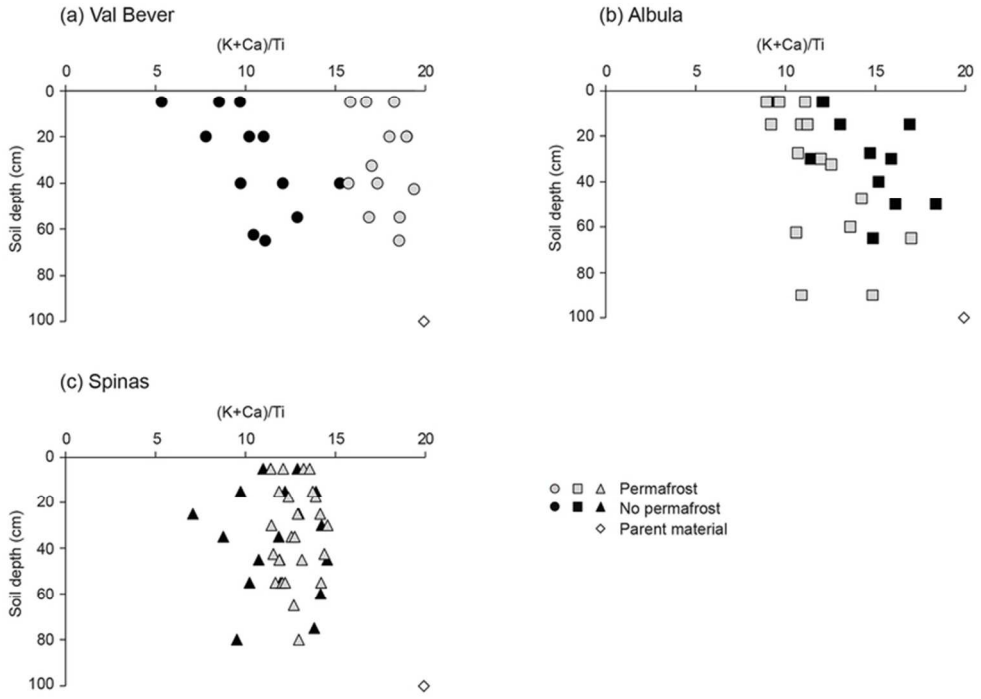

Figure 4

69x48mm (300 x 300 DPI)

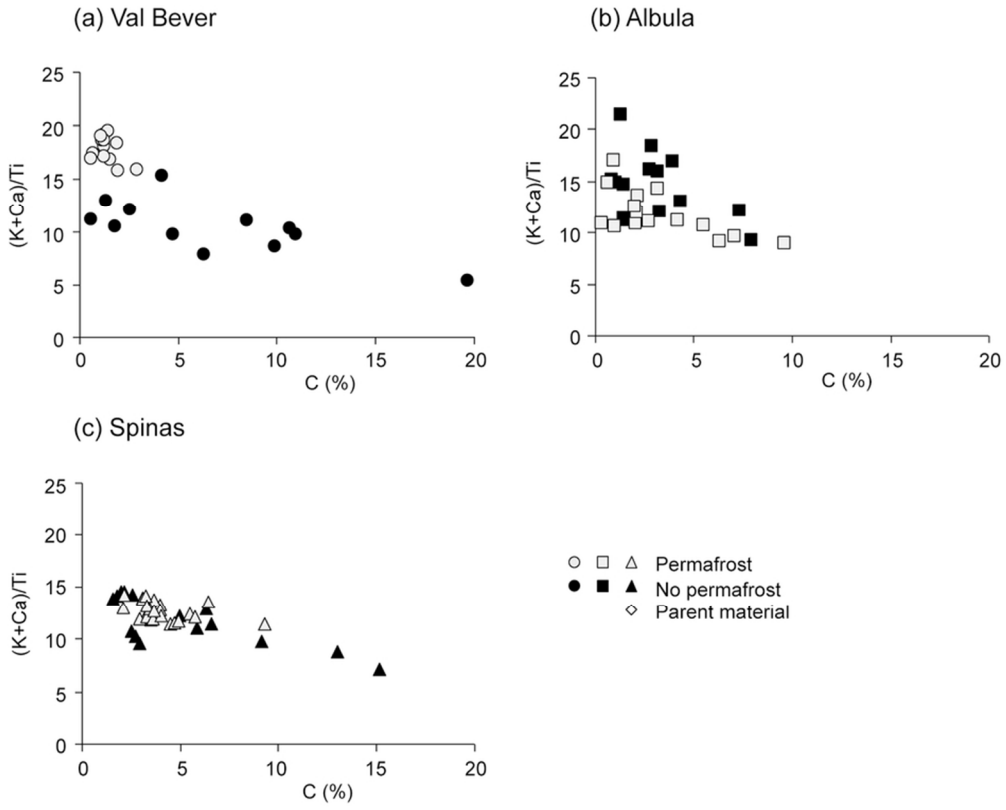

Figure 5

80x64mm (300 x 300 DPI)

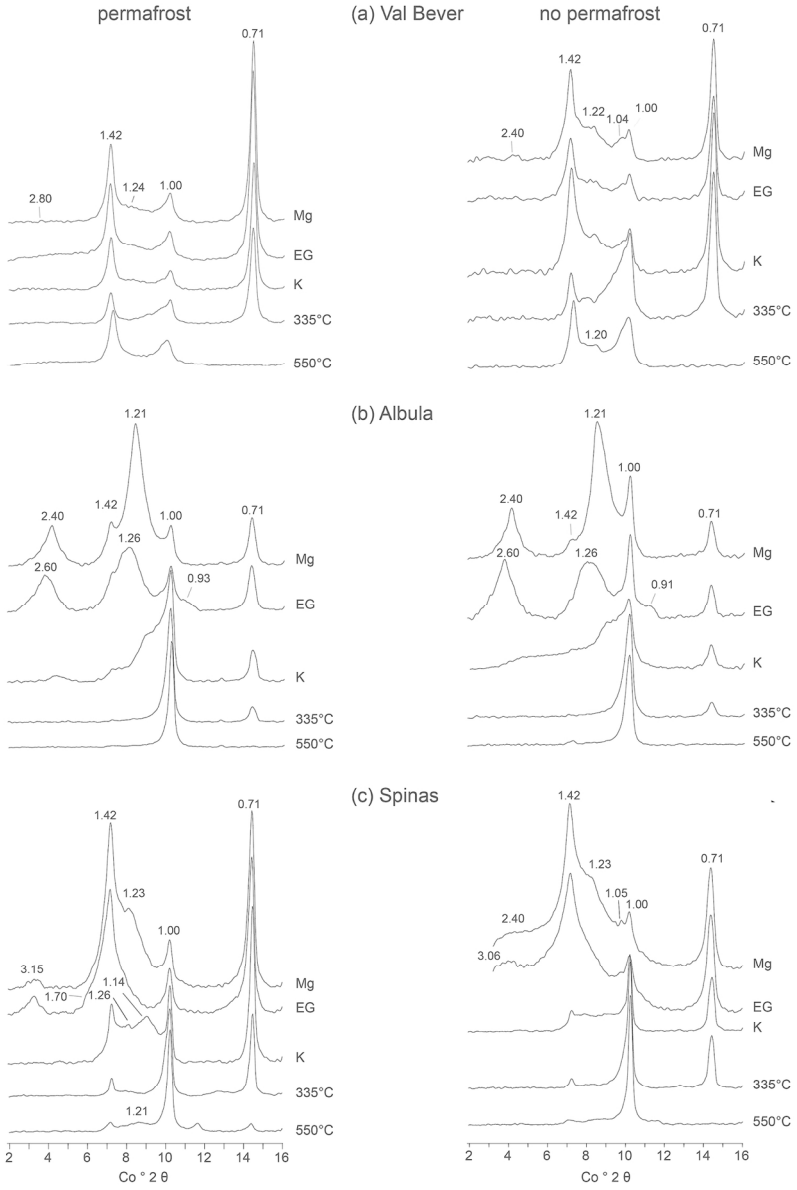

Figure 6

139x193mm (300 x 300 DPI)

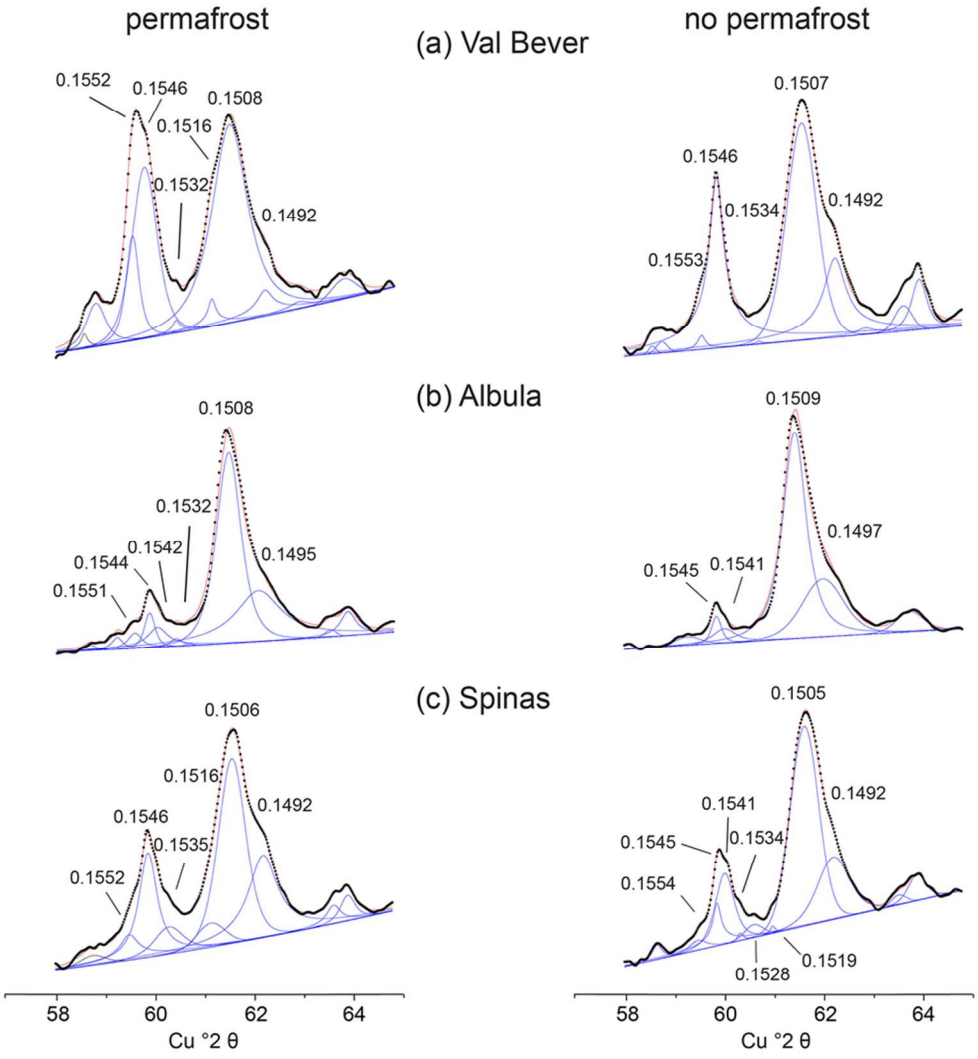

Figure 7

85x92mm (300 x 300 DPI)

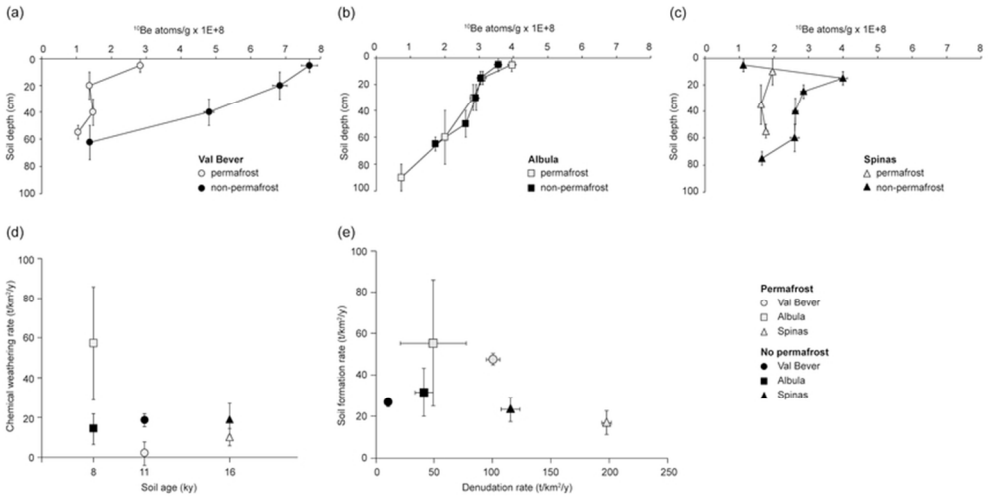

Figure 8

73x35mm (300 x 300 DPI)

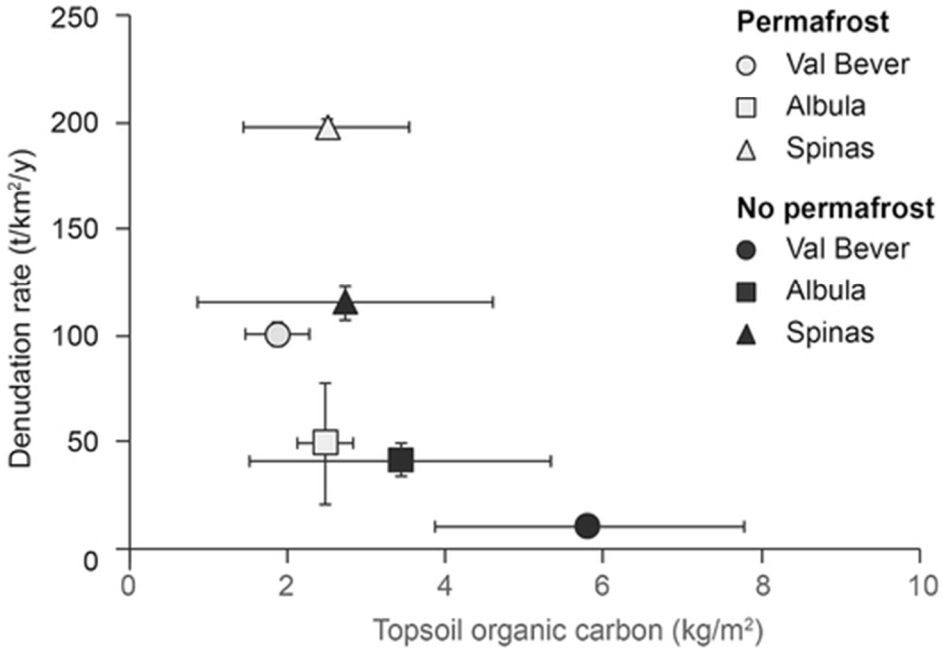

Figure 9

45x29mm (300 x 300 DPI)

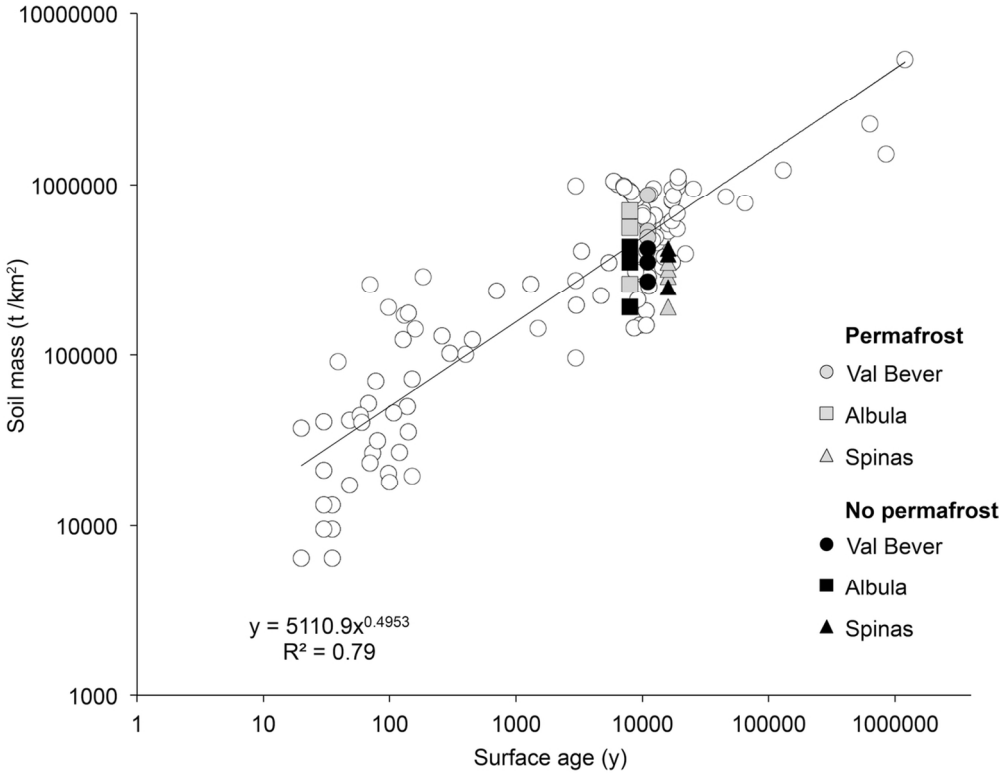

Figure 10

115x88mm (300 x 300 DPI)